Ultrasound in medicine and biology

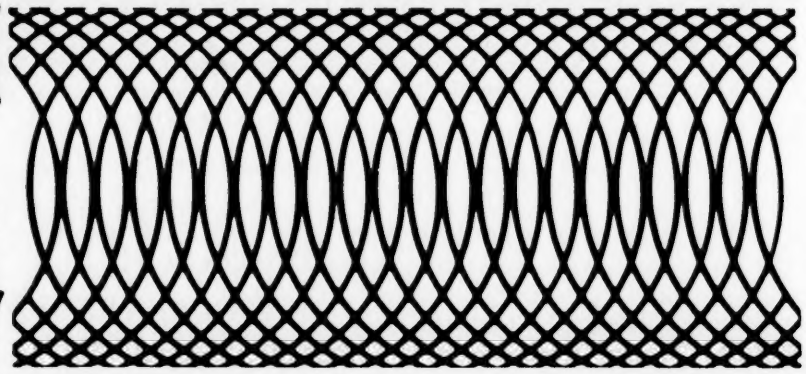

Supplement to *Ultrasound in Medicine and Biology,* Volume 23, Number 4, 1997

Author–Subject Index Volume 22 (1996)

Compiled by

Michael Halliwell

Department of Medical Physics, Bristol General Hospital, Bristol BS1 6SY, United Kingdom

ELSEVIER

ULTRASOUND IN MEDICINE AND BIOLOGY

WORLD FEDERATION FOR ULTRASOUND IN MEDICINE AND BIOLOGY

President: B. B. GOLDBERG, *USA*

Past-President: M. FUKUDA, *Japan*

President-Elect: H. LUTZ, *Germany*

Vice-President I: H. WATANABE, *Japan*

Vice-President II: D. E. ROBINSON, *Australia*

Treasurer: M. C. ZISKIN, *USA*

Secretary: S. HANCKE, *Denmark*

Administrative Councillors:

G. G. CERRI, *Brazil*

H. Y. CHEN, *Taiwan*

S. EIK-NES, *Norway*

C. R. B. MERRITT, *USA*

Co-opted Councillors:

C. A. BRUGUERA, *Argentina*

H. GHARBI, *Tunisia*

M. MAKUUCHI, *Japan*

Editor-in-Chief:

P. N. T. WELLS, *UK*

AFFILIATED SOCIETIES

American Institute of Ultrasound in Medicine (AIUM), A. B. Kurtz, Secretary, 14750 Sweitzer Lane, Suite 100, Laurel, MD 20707, USA

Asian Federation of Societies for Ultrasound in Medicine and Biology (AFSUMB), K. Nakayama, Secretary, Faculty of Science and Technology, Sophia University, 7-1 Kioicho, Chiyoda-ku, Tokyo, Japan

Australasian Society for Ultrasound in Medicine (ASUM), S. Butterworth, Executive Officer, 2/181 High Street, Willoughby, NSW 2068, Australia

European Federation of Societies for Ultrasound in Medicine and Biology (EFSUMB), E. Brown, General Secretary, 36 Portland Place, London W1N 3DG, UK

Latin-American Federation of Societies for Ultrasound in Medicine and Biology (FLAUS), G. G. Cerri, Permanent Secretary, Av. Paulista, 491 13° conj. 132, CEP 01311, São Paulo, Brazil

Mediterranean and African Society for Ultrasound (MASU), H. A. Gharbi, Secretary, 12 Ruc Mohamed Salahoddine, 1082 Tunis, Tunisia

Publishing Office: Elsevier Science Inc., 655 Avenue of the Americas, New York, NY 10010–5107, USA.

Please direct inquiries regarding advertising in this journal to Jay Allan Feinman, Advertising Sales Dept., Elsevier Science Inc., 655 Avenue of the Americas, New York, NY 10010-5107. Email: j.feinman@elsevier.com; Tel: (212) 633-3689; Fax: (212) 633-3820.

Published 9 per Annum. *Annual Institutional Subscription Rate* (1997): For customers in Europe, The CIS and Japan: Institutional Rate: NLG 1,215.00. Student/Resident Rate: NLG 101.00. For customers in all other Countries: Institutional Rate: US$750.00. Student/Resident Rate: US$62.00. Prices include postage and are subject to change without notice. Members of the World Federation for Ultrasound in Medicine and Biology may order personal subscriptions at a concessional rate; details of these rates are available upon request.

Any inquiry relating to subscriptions should be sent to: **The Americas:** Elsevier Science, Customer Support Department, P.O. Box 945, New York, NY 10010, USA. [Tel: (+1)212-633-3730/1-888 4ES-INFO. Fax: (+1)212-633-3680. E-mail: usinfo-f@elsevier.com]. **Japan:** Elsevier Science, Customer Support Department, 9-15 Higashi-Azabu 1-chome, Minato-ku, Tokyo 106, Japan [Tel: (+3)5561-5033. Fax: (+3)5561-5047. E-mail: kyf04035@niftyserve.or.jp]. **Asia Pacific (*excluding Japan*):** Elsevier Science (Singapore) Pte Ltd, No. 1 Temasek Avenue, 17-01 Millenia Tower, Singapore 039192. [Tel: (+65)434-3727. Fax: (+65)337-2230. E-mail: asiainfo@elsevier.com.sg]. **Rest of the World:** Elsevier Science, Customer Service Department, P.O. Box 211, 1001 AE Amsterdam, The Netherlands. [Tel: (+31)20-485-3757. Fax: (+31)20-485-3432. E-mail: nlinfo-f@elsevier.nl].

Please direct inquiries regarding the purchase of reprints to Dan Cronin, Elsevier Science Inc., 655 Avenue of the Americas, New York, NY 10010. Telephone: (212) 633-3813; Fax: (212) 633-3820.

ELSEVIER

Ultrasound in Med. & Biol., Vol. 23, Suppl., pp. 1–65, 1997
Copyright © 1997 World Federation for Ultrasound in Medicine & Biology
Printed in the USA. All rights reserved
0301-5629/97 $17.00 + .00

PII S0301-5629(97)00014-8

AUTHOR/SUBJECT INDEX

A

Ablation
ablation of tissue volumes using high intensity focused ultrasound (Malcolm), 659
interventional ultrasound (Holm), 773
physical characteristics and biological effects of laser-induced stress waves (Doukas), 151
the intensity dependence of the site of maximal energy deposition in focused ultrasound surgery (Watkin), 483

Ackerstaff, R. G. A., see van Swijndregt, A. D. M.

Acoustic emission
detection of acoustic emission from cavitation in tissue during clinical extracorporeal lithotripsy (Coleman), 1079

Acuff, J., see Dong, M.-L.

Acute CNS infection
transcranial Doppler sonography at the early stage of acute central nervous system infections in adults (Müller), 173

Adamson, S. L., see Surat, D. R.
Adamus, J., see Nowicki, A.
Adler, R. S., see Chen, J.-F.

Adnexal masses
a comparison of intratumoural indices of blood flow velocity and impedance for the diagnosis of ovarian cancer (Tailor), 837

Age related
increased stiffness of the aorta in children and adolescents with insulin-dependent diabetes mellitus (Hu), 537
nonlinear transcranial Doppler analysis demonstrates age-related changes of cerebral hemodynamics (Keunen), 383

Agglutination
measurement of antigen concentration by an ultrasound-enhanced latex immunoagglutination assay (Thomas), 1277

Akselrod, S., see Zimmer, Y.

Albunex
contrast-agent gas bodies enhance hemolysis induced by lithotripter shock waves and high-intensity focused ultrasound in whole blood (Miller), 1089

direct evidence of cavitation *in vivo* from diagnostic ultrasound (Holland), 917
hemolysis of Albunex-supplemented, 40% hematocrit human erythrocytes *in vitro* by 1-MHz pulsed ultrasound: acoustic pressure and pulse length dependence (Brayman), 927
pharmacokinetic studies of different echo-contrast agents in the cerebral circulation of dogs (Seidel), 1037

Alcohol injection
interventional ultrasound (Holm), 773

Alderman, J. L., see Holland, C. K.
Algazi, V. R., see Ferrara, K. W.
Allan, P. L.: clinical applications of Doppler ultrasound (2nd edition), 527 (Book Review)
Allard, L., Cloutier, G. and Durand, L.-G.: in response to Drs. Sensier and London, 365 (Letter)

Anaesthesia
transcranial Doppler ultrasonography in neurosurgery: effects of intracranial tumour on right middle cerebral artery flow velocity during induction of anaesthesia (Dong), 1163

Anayiotos, A. S., see Perry, G. J.
Anderson, T., see Lee, S.
Andreuccetti, F., see Capineri, L.

Angioplasty
computation of a location shift between two subsequent intravascular ultrasound registrations by cross-correlation analysis of the lumen area functions (Post), 239
in vitro validation of intravascular ultrasound imaging after balloon angioplasty of coronary artery stenosis (Peters), 999
interobserver reproducibility of qualitative and quantitative analysis of intravascular ultrasound images before and after peripheral balloon angioplasty (van der Lugt), 399
residual stenosis determined by intravascular ultrasound and duplex ultrasound after balloon angioplasty of the superficial femoral artery (Pasterkamp), 801
ultrasonic–pathologic comparison of postangioplasty myointimal hyperplasia and primary atheroma of the superficial femoral artery (Baumgartner), 815

Ankle/brachial index
ROC analysis of noninvasive tests for peripheral arterial disease (Lijmer), 391

Anlinker, M., see Bührer, A.

Antigen concentration
measurement of antigen concentration by an ultrasound-enhanced latex immunoagglutination assay (Thomas), 1277

Aorta
increased stiffness of the aorta in children and adolescents with insulin-dependent diabetes mellitus (Hu), 537

Apfel, R. E., see Deng, C. X.
Apfel, R. E., see Holland, C. K.

Apodisation
reduction of stress nonuniformities by apodization of compressor displacement in elastography (Konofagou), 1229

Armstrong, J., see Christopher, D. A.
Arnett, D., see Chambless, L. E.

Artefacts
differentiation between emboli and artefacts using dual-gated transcranial Doppler ultrasound (Smith), 1031
reduction of stress nonuniformities by apodization of compressor displacement in elastography (Konofagou), 1229
subtraction procedure for the registration of tissue perfusion with Doppler ultrasound (Bührer), 651
the effect of variations in transducer position and sound speed in intravascular ultrasound: a theoretical study (Thompson), 719

Arterial compliance
diameter and compliance in the human carotid artery — variations with age and sex (Reneman), 271 (Letter)
downstream determinants of pulsatility of the mean velocity waveform in the umbilical artery as predicted by a computer model (Surat), 707
in response to Drs. Reneman and Hoeks (Hensen), 273 (Letter)
increased stiffness of the aorta in children and adolescents with insulin-dependent diabetes mellitus (Hu), 537
new methods for arterial diameter measurement from B-mode images (Stadler), 25
the application of echo-tracking methods to endothelium-dependent vasoreactivity and arterial compliance measurements (Stadler), 35

Arterial diameter
a noninvasive method to estimate arterial impedance by means of assessment of local diameter change and the local center-line blood flow velocity using ultrasound (Brands), 895
diameter and compliance in the human carotid artery — variations with age and sex (Reneman), 271 (Letter)
in response to Drs. Reneman and Hoeks (Hensen), 273 (Letter)
new methods for arterial diameter measurement from B-mode images (Stadler), 25
the application of echo-tracking methods to endothelium-dependent vasoreactivity and arterial compliance measurements (Stadler), 35

Arterial distensibility
a noninvasive method to estimate arterial impedance by means of assessment of local diameter change and the local center-line blood flow velocity using ultrasound (Brands), 895
differentiation between emboli and artefacts using dual-gated transcranial Doppler ultrasound (Smith), 1031

Artery
a noninvasive method to estimate arterial impedance by means of assessment of local diameter change and the local center-line blood flow velocity using ultrasound (Brands), 895
accuracy of color Doppler velocity in the flow field proximal to a regurgitant orifice: implications for color Doppler quantitation of valvular incompetence (Perry), 605
an *in vitro* evaluation of the line pattern of the near and far walls of carotid arteries using B-mode ultrasound (van Swijndregt), 1007
assessment of temporal bias in longitudinal measurements of carotid intimal-medial thickness in the asymptomatic carotid artery progression study (ACAPS) (Riley), 405
colour duplex ultrasound assessment of lower limb arterial disease: the effect of adjacent disease (Sensier), 365 (Letter)
computation of a location shift between two subsequent intravascular ultrasound registrations by cross-correlation analysis of the lumen area functions (Post), 239
diameter and compliance in the human carotid artery — variations with age and sex (Reneman), 271 (Letter)
downstream determinants of pulsatility of the mean velocity waveform in the umbilical artery as predicted by a computer model (Surat), 707
in response to Drs. Reneman and Hoeks (Hensen), 273 (Letter)
in response to Drs. Sensier and London (Allard), 365 (Letter)
in vitro validation of intravascular ultrasound imaging after balloon angioplasty of coronary artery stenosis (Peters), 999
increased stiffness of the aorta in children and adolescents with insulin-dependent diabetes mellitus (Hu), 537
interobserver reproducibility of qualitative and quantitative analysis of intravascular ultrasound images before and after peripheral balloon angioplasty (van der Lugt), 399
new methods for arterial diameter measurement from B-mode images (Stadler), 25
noninvasive arterial occlusion using MRI-guided focused ultrasound (Hynynen), 1071
nonlinear transcranial Doppler analysis demonstrates age-related changes of cerebral hemodynamics (Keunen), 383
observer variability in volumetric blood flow measurements in leg arteries using duplex ultrasound (Hussain), 287
pitfalls in the diagnosis of origin stenosis of the coeliac and superior mesenteric arteries with transabdominal colour duplex examination (Geelkerken), 695
power Doppler: an advance over colour Doppler for transcranial imaging? (Kenton), 313
reproducibility of extracranial carotid atherosclerotic lesions assessed by B-mode ultrasound: the atherosclerosis risk in communities study (Li), 791
residual stenosis determined by intravascular ultrasound and duplex ultrasound after balloon angioplasty of the superficial femoral artery (Pasterkamp), 801
temporal correlation of blood scattering signals *in vivo* from radiofrequency intravascular ultrasound (Li), 583
the effect of variations in transducer position and sound speed in intravascular ultrasound: a theoretical study (Thompson), 719

the influence of acoustic impedance mismatch on poststenotic pulsed-Doppler ultrasound measurements in a coronary artery model (Jones), 623
three-dimensional ultrasonic angiography using power-mode Doppler (Ritchie), 277
ultrasonic–pathologic comparison of postangioplasty myointimal hyperplasia and primary atheroma of the superficial femoral artery (Baumgartner), 815
variability in B-mode ultrasound measurements in the atherosclerosis risk in communities (ARIC) study (Chambless), 545

Aspiration
interventional ultrasound (Holm), 773
physics of ultrasonic surgery using tissue fragmentation: part I (Cimino), 89

Arterial impedance
a noninvasive method to estimate arterial impedance by means of assessment of local diameter change and the local center-line blood flow velocity using ultrasound (Brands), 895

Arteriovenous fistula
diagnosis and follow-up of carotid-cavernous fistulas by carotid duplex sonography and transcranial color Doppler imaging (Chen), 1155

Atherosclerosis
an *in vitro* evaluation of the line pattern of the near and far walls of carotid arteries using B-mode ultrasound (van Swijndregt), 1007
assessment of temporal bias in longitudinal measurements of carotid intimal-medial thickness in the asymptomatic carotid artery progression study (ACAPS) (Riley), 405
computation of a location shift between two subsequent intravascular ultrasound registrations by cross-correlation analysis of the lumen area functions (Post), 239
interobserver reproducibility of qualitative and quantitative analysis of intravascular ultrasound images before and after peripheral balloon angioplasty (van der Lugt), 399
new methods for arterial diameter measurement from B-mode images (Stadler), 25
observer variability in volumetric blood flow measurements in leg arteries using duplex ultrasound (Hussain), 287
pitfalls in the diagnosis of origin stenosis of the coeliac and superior mesenteric arteries with transabdominal colour duplex examination (Geelkerken), 695
reproducibility of extracranial carotid atherosclerotic lesions assessed by B-mode ultrasound: the atherosclerosis risk in communities study (Li), 791
residual stenosis determined by intravascular ultrasound and duplex ultrasound after balloon angioplasty of the superficial femoral artery (Pasterkamp), 801
ROC analysis of noninvasive tests for peripheral arterial disease (Lijmer), 391
the application of echo-tracking methods to endothelium-dependent vasoreactivity and arterial compliance measurements (Stadler), 35
the effect of variations in transducer position and sound speed in intravascular ultrasound: a theoretical study (Thompson), 719

three-dimensional power Doppler imaging: a phantom study to quantify vessel stenosis (Guo), 1059
variability in B-mode ultrasound measurements in the atherosclerosis risk in communities (ARIC) study (Chambless), 545

Attenuation
amplitude, isobar and grey-scale imaging of ultrasonic shadows behind rigid, elastic and gaseous spheres (Filipczynski), 261
factors affecting the ultrasonic properties of equine digital flexor tendons (Miles), 907
influence of tissue preparation on the high-frequency acoustic properties of normal kidney tissue (Sasaki), 1261
precision and accuracy of acoustospectrographic parameters (Huisman), 855
quantitative ultrasonic diagnosis of silicone breast implant rupture: an *in vitro* feasibility study (Forsberg), 53
simulation of ultrasonic imaging with linear arrays in causal absorptive media (Berkhoff), 245
some considerations on the measurements of mean frequency shift and integrated backscatter following administration of Albunex (Wang), 441

Autocorrelation
autocorrelation of integrated power Doppler signals and its application (Chen), 1053

Automated waveform analysis
evaluation of an automated real-time spectral analysis technique (Rickey), 61

Azadniv, M., see Brayman, A. A.

B

B-mode imaging
assessment of temporal bias in longitudinal measurements of carotid intimal-medial thickness in the asymptomatic carotid artery progression study (ACAPS) (Riley), 405
new methods for arterial diameter measurement from B-mode images (Stadler), 25
spatial compounding in ultrasonic imaging using an articulated scan arm (Hernandez), 229
studies on the use of non-Rayleigh statistics for ultrasonic tissue characterization (Shankar), 873
variability in B-mode ultrasound measurements in the atherosclerosis risk in communities (ARIC) study (Chambless), 545

van Baalen, J. M., see Delahunt, T. A.
van Baalen, J. M., see Geelkerken, R. H.

Backscatter
analysis of transmural trend of myocardial integrated ultrasonic backscatter in patients with old myocardial infarction (Naito), 807
autocorrelation of integrated power Doppler signals and its application (Chen), 1053

cyclic variation of Doppler power from whole blood under pulsatile flow (Wu), 883
factors affecting the ultrasonic properties of equine digital flexor tendons (Miles), 907
influence of preload, afterload and contractility on myocardial ultrasonic tissue characterization with integrated backscatter (Naito), 305
particle and voxel approaches for simulating ultrasound backscattering from tissue (Lim), 1237
precision and accuracy of acoustospectrographic parameters (Huisman), 855
quantitative ultrasonic diagnosis of silicone breast implant rupture: an *in vitro* feasibility study (Forsberg), 53
some considerations on the measurements of mean frequency shift and integrated backscatter following administration of Albunex (Wang), 441
studies on the use of non-Rayleigh statistics for ultrasonic tissue characterization (Shankar), 873
temporal correlation of blood scattering signals *in vivo* from radiofrequency intravascular ultrasound (Li), 583
the distribution of the local entropy in ultrasound images (Zimmer), 431
the relationship between myocardial integrated backscatter, perfusion pressure and wall thickness during isovolumic contraction: an isolated pig heart study (Rijsterborgh), 43
ultrasonic measurement of glomerular diameters in normal adult humans (Hall), 987
ultrasound backscatter microscope analysis of mouse melanoma progression (Turnbull), 845

Bacon, D. R., see Shaw, A.
Baggs, R., Penney, D. P., Cox, C., Child, S. Z., Raeman, C. H., Dalecki, D. and Carstensen, E. L.: thresholds for ultrasonically induced lung hemorrhage in neonatal swine, 119
Balcer-Kubiczek, E. K., see Harrison, G. H.

Balloon angioplasty
in vitro validation of intravascular ultrasound imaging after balloon angioplasty of coronary artery stenosis (Peters), 999
spatial compounding in ultrasonic imaging using an articulated scan arm (Hernandez), 229

Bascom, P. A. J., see Lim, B.
Basset, O., see Hernandez, A.
Bates, J.: manual of diagnostic ultrasound, 767
Baumgartner, I., Redha, F., Baumgartner, R. W., Do, D.-D. and Mahler, F.: ultrasonic–pathologic comparison of postangioplasty myointimal hyperplasia and primary atheroma of the superficial femoral artery, 815
Baumgartner, R. W., see Baumgartner, I.

Beam plots
accuracy of color Doppler velocity in the flow field proximal to a regurgitant orifice: implications for color Doppler quantitation of valvular incompetence (Perry), 605
cyclic variation of Doppler power from whole blood under pulsatile flow (Wu), 883

the influence of acoustic impedance mismatch on poststenotic pulsed-Doppler ultrasound measurements in a coronary artery model (Jones), 623
the intensity dependence of the site of maximal energy deposition in focused ultrasound surgery (Watkin), 483
ultrasound surgery using multiple sonications — treatment time considerations (Fan), 471

Bell, P. R. F., see Smith, J. L.
Beller, K.-D., see Seidel, G.
Bellotti, M., see Pennati, G.
Berger, B., see Giller, C. A.
Berkhoff, A. P., Thijssen, J. M. and Homan, R. J. F.: simulation of ultrasonic imaging with linear arrays in causal absorptive media, 245
Bertrand, M., see Kallel, F.
Bezante, G. P., see Schwarz, K. Q.

Bio-heat transfer
perfusion corrections for ultrasonic heating in nonperfused media (Shaw), 203

Bioeffects
A review of *in vitro* bioeffects of inertial ultrasonic cavitation from a mechanistic perspective (Miller), 1131
a test for cavitation as a mechanism for intestinal hemorrhage in mice exposed to a piezoelectric lithotripter (Dalecki), 493
ablation of tissue volumes using high intensity focused ultrasound (Malcolm), 659
alteration of cell membrane by stress waves *in vitro* (Lee), 1285
application of focused ultrasound for the stimulation of neural structures (Gavrilov), 179
biophysical effects of high-energy pulsed ultrasound on human cells (Feigl), 1267
cell-type-specific response to shock waves of suspended or pelleted cells as analysed by flow cytometry or electrical cell volume determination (Endl), 515
contrast-agent gas bodies enhance hemolysis induced by lithotripter shock waves and high-intensity focused ultrasound in whole blood (Miller), 1089
direct evidence of cavitation *in vivo* from diagnostic ultrasound (Holland), 917
disturbance of cellular calcium homeostasis by *in vitro* application of shock waves (Suhr), 671
exposure-time dependence of the threshold for ultrasonically induced murine lung hemorrhage (Raeman), 139
hemolysis of Albunex-supplemented, 40% hematocrit human erythrocytes *in vitro* by 1-MHz pulsed ultrasound: acoustic pressure and pulse length dependence (Brayman), 927
in vitro measurements of inertial cavitation thresholds in human blood (Deng), 939
in vitro mechanisms of chemopotentiation by tone-burst ultrasound (Harrison), 355
noninvasive arterial occlusion using MRI-guided focused ultrasound (Hynynen), 1071

physical characteristics and biological effects of laser-induced stress waves (Doukas), 151
potential adverse effects of high-intensity focused ultrasound exposure on blood vessels *in vivo* (Hynynen), 193
rabbit and pig lung damage comparison from exposure to continuous wave 30-kHz ultrasound (O'Brien), 345
re-evaluation of the concept that high cell concentrations "protect" cells *in vitro* from ultrasonically induced lysis (Brayman), 497
the influence of high-energy shock waves on the development of metastases (Oosterhof), 339
the intensity dependence of the site of maximal energy deposition in focused ultrasound surgery (Watkin), 483
the role of cavitation in the induction of cellular DNA damage by ultrasound and lithotripter shock waves *in vitro* (Miller), 681
thresholds for ultrasonically induced lung hemorrhage in neonatal swine (Baggs), 119
ultrasound surgery using multiple sonications — treatment time considerations (Fan), 471

Biopsy
biopsy of nonpalpable cervical lymph nodes: selection criteria for ultrasound-guided biopsy in patients with head and neck squamous cell carcinoma (Kruyt), 413
interventional ultrasound (Holm), 773
noninvasive arterial occlusion using MRI-guided focused ultrasound (Hynynen), 1071
ultrasound-guided spleen biopsy in chimpanzees (pan troglodytes) (Eder), 19

Birch, H. L., see Miles, C. A.

Bladder cancer
the combined effects of high-energy shock waves and ionising radiation on a human bladder cancer cell line (Fickweiler), 1097

Bland, M., see Hussain, S. T.

Blood flow
a high-frequency continuous-wave Doppler ultrasound system for the detection of blood flow in the microcirculation (Christopher), 1991
a noninvasive method to estimate arterial impedance by means of assessment of local diameter change and the local center-line blood flow velocity using ultrasound (Brands), 895
an impedance index in normal subjects and in subarachnoid hemorrhage (Giller), 373
changes in superior mesenteric artery Doppler waveform during reduction of cardiac stroke volume and hypotension (Perko), 11
comparison of trans- and intra-abdominal duplex examinations of the splanchnic circulation (Delahunt), 165
computational analysis of the ductus venosus fluid dynamics based on Doppler measurements (Pennati), 1017
cyclic variation of Doppler power from whole blood under pulsatile flow (Wu), 883
development of quantitative Doppler indices for uteroplacental and fetal blood flow during the third trimester (Joern), 823

diagnosis and follow-up of carotid-cavernous fistulas by carotid duplex sonography and transcranial color Doppler imaging (Chen), 1155
downstream determinants of pulsatility of the mean velocity waveform in the umbilical artery as predicted by a computer model (Surat), 707
high resolution 3D color flow mapping: applied to the assessment of breast vasculature (Ferrara), 293
observer variability in volumetric blood flow measurements in leg arteries using duplex ultrasound (Hussain), 287
pitfalls in the diagnosis of origin stenosis of the coeliac and superior mesenteric arteries with transabdominal colour duplex examination (Geelkerken), 695
subtraction procedure for the registration of tissue perfusion with Doppler ultrasound (Bührer), 651
the Doppler kinetics of microbubble echo contrast (Schwarz), 453
three-dimensional ultrasonic angiography using power-mode Doppler (Ritchie), 277
transcranial Doppler sonography at the early stage of acute central nervous system infections in adults (Müller), 173
transcranial Doppler ultrasonography in neurosurgery: effects of intracranial tumour on right middle cerebral artery flow velocity during induction of anaesthesia (Dong), 1163
ultrasound guided spleen biopsy in chimpanzees (pan troglodytes) (Eder), 19
velocity vector reconstruction for color flow Doppler: experimental evaluation of a new geometrical method (Giarré), 75
volumetric flow estimation *in vivo* and *in vitro* using pulsed-Doppler ultrasound (Holland), 591

Blood pressure
an impedance index in normal subjects and in subarachnoid hemorrhage (Giller), 373
computational analysis of the ductus venosus fluid dynamics based on Doppler measurements (Pennati), 1017

Blood scattering
cyclic variation of Doppler power from whole blood under pulsatile flow (Wu), 883
temporal correlation of blood scattering signals *in vivo* from radiofrequency intravascular ultrasound (Li), 583

Blood vessels
a noninvasive method to estimate arterial impedance by means of assessment of local diameter change and the local center-line blood flow velocity using ultrasound (Brands), 895
accuracy of color Doppler velocity in the flow field proximal to a regurgitant orifice: implications for color Doppler quantitation of valvular incompetence (Perry), 605
an *in vitro* evaluation of the line pattern of the near and far walls of carotid arteries using B-mode ultrasound (van Swijndregt), 1007
assessment of temporal bias in longitudinal measurements of carotid intimal-medial thickness in the asymptomatic carotid artery progression study (ACAPS) (Riley), 405
colour duplex ultrasound assessment of lower limb arterial disease: the effect of adjacent disease (Sensier), 365 (Letter)

computation of a location shift between two subsequent intravascular ultrasound registrations by cross-correlation analysis of the lumen area functions (Post), 239
diameter and compliance in the human carotid artery — variations with age and sex (Reneman), 271 (Letter)
downstream determinants of pulsatility of the mean velocity waveform in the umbilical artery as predicted by a computer model (Surat), 707
in response to Drs. Reneman and Hoeks (Hensen), 273 (Letter)
in response to Drs. Sensier and London (Allard), 365 (Letter)
in vitro validation of intravascular ultrasound imaging after balloon angioplasty of coronary artery stenosis (Peters), 999
increased stiffness of the aorta in children and adolescents with insulin-dependent diabetes mellitus (Hu), 537
interobserver reproducibility of qualitative and quantitative analysis of intravascular ultrasound images before and after peripheral balloon angioplasty (van der Lugt), 399
new methods for arterial diameter measurement from B-mode images (Stadler), 25
noninvasive arterial occlusion using MRI-guided focused ultrasound (Hynynen), 1071
nonlinear transcranial Doppler analysis demonstrates age-related changes of cerebral hemodynamics (Keunen), 383
observer variability in volumetric blood flow measurements in leg arteries using duplex ultrasound (Hussain), 287
pitfalls in the diagnosis of origin stenosis of the coeliac and superior mesenteric arteries with transabdominal colour duplex examination (Geelkerken), 695
potential adverse effects of high-intensity focused ultrasound exposure on blood vessels *in vivo* (Hynynen), 193
power Doppler: an advance over colour Doppler for transcranial imaging? (Kenton), 313
reproducibility of extracranial carotid atherosclerotic lesions assessed by B-mode ultrasound: the atherosclerosis risk in communities study (Li), 791
residual stenosis determined by intravascular ultrasound and duplex ultrasound after balloon angioplasty of the superficial femoral artery (Pasterkamp), 801
temporal correlation of blood scattering signals *in vivo* from radiofrequency intravascular ultrasound (Li), 583
the effect of variations in transducer position and sound speed in intravascular ultrasound: a theoretical study (Thompson), 719
the influence of acoustic impedance mismatch on poststenotic pulsed-Doppler ultrasound measurements in a coronary artery model (Jones), 623
three-dimensional power Doppler imaging: a phantom study to quantify vessel stenosis (Guo), 1059
three-dimensional ultrasonic angiography using power-mode Doppler (Ritchie), 277
ultrasonic–pathologic comparison of postangioplasty myointimal hyperplasia and primary atheroma of the superficial femoral artery (Baumgartner), 815
variability in B-mode ultrasound measurements in the atherosclerosis risk in communities (ARIC) study (Chambless), 545

Bloomfield, T. S., see Turnbull, D. H.
van Bockel, J. H., see Delahunt, T. A.
de Boer, M. F., see Kruyt, R. H.
Bom, N., see Djoa, K. K.
Bom, N., see Li, W.
Bom, N., see van der Lugt, A.
Bom, N., see Rijsterborgh, H.
Bom, N., see van Swijndregt, A. D. M.
Bond, L. J. and Cimino, W. W.: physics of ultrasonic surgery using tissue fragmentation: part II, 101
Bond, L. J., see Cimino, W. W.
Borst, C., see Pasterkamp, G.
Borst, C., see Post, M. J.
Bos, L. J., Piek, J. J. and Spaan, J. A. E.: effects of shadowing on the time–intensity curves in contrast echocardiography: a phantom study, 217
Bourne, T. H., see Tailor, A.

Brachytherapy
interventional ultrasound (Holm), 773

Brain edema
transcranial Doppler sonography at the early stage of acute central nervous system infections in adults (Müller), 173

Brands, P. J., Hoeks, A. P. G., Rutten, M. C. M. and Reneman, R. S.: a noninvasive method to estimate arterial impedance by means of assessment of local diameter change and the local center-line blood flow velocity using ultrasound, 895
Brayman, A. A., Azadniv, M., Cox, C. and Miller, M. W.: hemolysis of Albunex-supplemented, 40% hematocrit human erythrocytes *in vitro* by 1-MHz pulsed ultrasound: acoustic pressure and pulse length dependence, 927
Brayman, A. A., Church, C. C. and Miller, M. W.: re-evaluation of the concept that high cell concentrations "protect" cells *in vitro* from ultrasonically induced lysis, 497
Brayman, A. A., see Miller, M. W.

Breast
high resolution 3D color flow mapping: applied to the assessment of breast vasculature (Ferrara), 293
quantitative ultrasonic diagnosis of silicone breast implant rupture: an *in vitro* feasibility study (Forsberg), 53
studies on the use of non-Rayleigh statistics for ultrasonic tissue characterization (Shankar), 873

Breast implants
quantitative ultrasonic diagnosis of silicone breast implant rupture: an *in vitro* feasibility study (Forsberg), 53

Brümmer, F., see Suhr, D.
Bührer, A., Moser, U. T., Schumacher, P. M., Pasch, T. and Anlinker, M.: subtraction procedure for the registration of tissue perfusion with Doppler ultrasound, 651
Burns, P. N., see Christopher, D. A.

C

Cai, J., see Li, R.

Calcium
disturbance of cellular calcium homeostasis by *in vitro* application of shock waves (Suhr), 671

Callipers
the importance of rigorous testing of circumference measuring callipers (Dudley), 1117

Campbell, S., see Tailor, A.

Cancer
ablation of tissue volumes using high intensity focused ultrasound (Malcolm), 659

Cape, E. G., Sung, H.-W. and Yoganathan, A. P.: hemodynamic assessment of carbomedics bileaflet heart valves by ultrasound: studies in the aortic and mitral positions, 421
Capineri, L., Masotti, L., Rocchi, S., Andreuccetti, F., Cerofolini, M. and Tondini, A.: nearly real-time visualization of arbitrary two-dimensional sections from three-dimensional acquisition, 319

Cardiac stroke volume
changes in superior mesenteric artery Doppler waveform during reduction of cardiac stroke volume and hypotension (Perko), 11

Cardinal, H. N., see Tong, S.

Cardiology
accuracy of color Doppler velocity in the flow field proximal to a regurgitant orifice: implications for color Doppler quantitation of valvular incompetence (Perry), 605
analysis of transmural trend of myocardial integrated ultrasonic backscatter in patients with old myocardial infarction (Naito), 807
assessment of wall velocity gradient imaging using a test phantom (Nowicki), 1255
effects of shadowing on the time–intensity curves in contrast echocardiography: a phantom study (Bos), 217
influence of preload, afterload and contractility on myocardial ultrasonic tissue characterization with integrated backscatter (Naito), 305
nearly real-time visualization of arbitrary two-dimensional sections from three-dimensional acquisition (Capineri), 319
the Doppler kinetics of microbubble echo contrast (Schwarz), 453
the influence of acoustic impedance mismatch on poststenotic pulsed-Doppler ultrasound measurements in a coronary artery model (Jones), 623
the relationship between myocardial integrated backscatter, perfusion pressure and wall thickness during isovolumic contraction: an isolated pig heart study (Rijsterborgh), 43
two decades of transesophageal phased array probes (Djoa), 1
verification of cardiac Doppler tissue images using grey-scale M-mode images (Fleming), 573

Carotid artery
an *in vitro* evaluation of the line pattern of the near and far walls of carotid arteries using B-mode ultrasound (van Swijndregt), 1007
assessment of temporal bias in longitudinal measurements of carotid intimal-medial thickness in the asymptomatic carotid artery progression study (ACAPS) (Riley), 405
diagnosis and follow-up of carotid-cavernous fistulas by carotid duplex sonography and transcranial color Doppler imaging (Chen), 1155
diameter and compliance in the human carotid artery — variations with age and sex (Reneman), 271 (Letter)
differentiation between emboli and artefacts using dual-gated transcranial Doppler ultrasound (Smith), 1031
in response to Drs. Reneman and Hoeks (Hensen), 273 (Letter)
reproducibility of extracranial carotid atherosclerotic lesions assessed by B-mode ultrasound: the atherosclerosis risk in communities study (Li), 791
the application of echo-tracking methods to endothelium-dependent vasoreactivity and arterial compliance measurements (Stadler), 35
variability in B-mode ultrasound measurements in the atherosclerosis risk in communities (ARIC) study (Chambless), 545
velocity vector reconstruction for color flow Doppler: experimental evaluation of a new geometrical method (Giarré), 75

Carson, P. L., see Chen, J.-F.
Carstensen, E. L., see Baggs, R.
Carstensen, E. L., see Christopher, T.
Carstensen, E. L., see Dalecki, D.
Carstensen, E. L., see see Raeman, C. H.

Causal absorptive media
simulation of ultrasonic imaging with linear arrays in causal absorptive media (Berkhoff), 245

Cavitation
a new method of quantitative cavitation assessment in the field of a lithotripter (Jöchle), 329
a review of *in vitro* bioeffects of inertial ultrasonic cavitation from a mechanistic perspective (Miller), 1131
a test for cavitation as a mechanism for intestinal hemorrhage in mice exposed to a piezoelectric lithotripter (Dalecki), 493
biophysical effects of high-energy pulsed ultrasound on human cells (Feigl), 1267
detection of acoustic emission from cavitation in tissue during clinical extracorporeal lithotripsy (Coleman), 1079
direct evidence of cavitation *in vivo* from diagnostic ultrasound (Holland), 917
disturbance of cellular calcium homeostasis by *in vitro* application of shock waves (Suhr), 671
in vitro measurements of inertial cavitation thresholds in human blood (Deng), 939
physics of ultrasonic surgery using tissue fragmentation: part I (Cimino), 89
the intensity dependence of the site of maximal energy deposition in focused ultrasound surgery (Watkin), 483

the role of cavitation in the induction of cellular DNA damage by ultrasound and lithotripter shock waves *in vitro* (Miller), 681

Celiac artery
comparison of trans- and intra-abdominal duplex examinations of the splanchnic circulation (Delahunt), 165

Cell lysis
a review of *in vitro* bioeffects of inertial ultrasonic cavitation from a mechanistic perspective (Miller), 1131
biophysical effects of high-energy pulsed ultrasound on human cells (Feigl), 1267
contrast-agent gas bodies enhance hemolysis induced by lithotripter shock waves and high-intensity focused ultrasound in whole blood (Miller), 1089
hemolysis of Albunex-supplemented, 40% hematocrit human erthrocytes *in vitro* by 1-MHz pulsed ultrasound: acoustic pressure and pulse length dependence (Brayman), 927
re-evaluation of the concept that high cell concentrations "protect" cells *in vitro* from ultrasonically induced lysis (Brayman), 497
the combined effects of high-energy shock waves and ionising radiation on a human bladder cancer cell line (Fickweiler), 1097

Cell viability
cell-type-specific response to shock waves of suspended or pelleted cells as analysed by flow cytometry or electrical cell volume determination (Endl), 515
contrast-agent gas bodies enhance hemolysis induced by lithotripter shock waves and high-intensity focused ultrasound in whole blood (Miller), 1089
disturbance of cellular calcium homeostasis by *in vitro* application of shock waves (Suhr), 671
hemolysis of Albunex-supplemented, 40% hematocrit human erthrocytes *in vitro* by 1-MHz pulsed ultrasound: acoustic pressure and pulse length dependence (Brayman), 927
in vitro mechanisms of chemopotentiation by tone-burst ultrasound (Harrison), 355
physical characteristics and biological effects of laser-induced stress waves (Doukas), 151
re-evaluation of the concept that high cell concentrations "protect" cells *in vitro* from ultrasonically induced lysis (Brayman), 497
the role of cavitation in the induction of cellular DNA damage by ultrasound and lithotripter shock waves *in vitro* (Miller), 681

Cellularity
factors affecting the ultrasonic properties of equine digital flexor tendons (Miles), 907

Cerebral flow
an impedance index in normal subjects and in subarachnoid hemorrhage (Giller), 373
development of quantitative Doppler indices for uteroplacental and fetal blood flow during the third trimester (Joern), 823
nonlinear transcranial Doppler analysis demonstrates age-related changes of cerebral hemodynamics (Keunen), 383

pharmacokinetic studies of different echo-contrast agents in the cerebral circulation of dogs (Seidel), 1037
power Doppler: an advance over colour Doppler for transcranial imaging? (Kenton), 313
transcranial Doppler sonography at the early stage of acute central nervous system infections in adults (Müller), 173
transcranial Doppler ultrasonography in neurosurgery: effects of intracranial tumour on right middle cerebral artery flow velocity during induction of anaesthesia (Dong), 1163

Cerofolini, M., see Capineri, L.
Céspedes, I., see Konofagou, E.
Céspedes, I., see Varghese, T.
Chambless, L. E., Zhong, M. M., Arnett, D., Folsom, A. R., Riley, W. A. and Heiss, G.: variability in B-mode ultrasound measurements in the atherosclerosis risk in communities (ARIC) study, 545
Chang, P. H., see Wang, S. H.
Chang, P. H., Shung, K. K. and Levene, H. B.: quantitative measurements of second harmonic Doppler using ultrasound contrast agents, 1205
Chang, Y.-C., see Chen, Y.-W.

Characterisation
an *in vitro* evaluation of the line pattern of the near and far walls of carotid arteries using B-mode ultrasound (van Swijndregt), 1007
analysis of transmural trend of myocardial integrated ultrasonic backscatter in patients with old myocardial infarction (Naito), 807
estimating tissue strain from signal decorrelation using the correlation coefficient (Varghese), 1249
factors affecting the ultrasonic properties of equine digital flexor tendons (Miles), 907
in vitro validation of intravascular ultrasound imaging after balloon angioplasty of coronary artery stenosis (Peters), 999
influence of preload, afterload and contractility on myocardial ultrasonic tissue characterization with integrated backscatter (Naito), 305
influence of tissue preparation on the high-frequency acoustic properties of normal kidney tissue (Sasaki), 1261
particle and voxel approaches for simulating ultrasound backscattering from tissue (Lim), 1237
physics of ultrasonic surgery using tissue fragmentation: part I (Cimino), 89
precision and accuracy of acoustospectrographic parameters (Huisman), 855
real-time assessment of the parameter of nonlinearity in tissue using "nonlinear shadowing" (Fatemi), 1215
studies on the use of non-Rayleigh statistics for ultrasonic tissue characterization (Shankar), 873
ultrasonic measurement of glomerular diameters in normal adult humans (Hall), 987
ultrasonic–pathologic comparison of postangioplasty myointimal hyperplasia and primary atheroma of the superficial femoral artery (Baumgartner), 815

Chatzimavroudis, G. P., see Jones, S. A.

Chemopotentiation
in vitro mechanisms of chemopotentiation by tone-burst ultrasound (Harrison), 355

Chen, J.-F., Fowlkes, J. B., Carson, P. L., Rubin, J. M. and Adler, R. S.: autocorrelation of integrated power Doppler signals and its application, 1053
Chen, X., see Schwarz, K. Q.
Chen, Y.-W., Jeng, J.-S., Liu, H.-M., Yip, P.-K., Hwang, B.-S., Lin, W.-H., Chang, Y.-C. and Tu, Y.-K.: diagnosis and follow-up of carotid-cavernous fistulas by carotid duplex sonography and transcranial color Doppler imaging, 1155
Child, S. Z., see Baggs, R.
Child, S. Z., see Dalecki, D.
Child, S. Z., see Raeman, C. H.

Chimpanzee
ultrasound guided spleen biopsy in chimpanzees (pan troglodytes) (Eder), 19

Chirossel, P., see Hernandez, A.
Chiu, W., see Hughes, S. W.

CHO cells
in vitro mechanisms of chemopotentiation by tone-burst ultrasound (Harrison), 355

Choi, M. J., see Coleman, A. J.
Christopher, D. A., Burns, P. N., Armstrong, J. and Foster, F. S.: a high-frequency continuous-wave Doppler ultrasound system for the detection of blood flow in the microcirculation, 1991
Christopher, T. and Carstensen, E. L.: finite amplitude distortion and its relationship to linear derating formulae for diagnostic ultrasound systems, 1103
Chung, A., see Hynynen, K.
Chung, A. H., see Hynynen, K.
Church, C. C., see Brayman, A. A.
Cimino, W. W. and Bond, L. J.: physics of ultrasonic surgery using tissue fragmentation: part I, 89
Cimino, W. W., see Bond, L. J.
Clancy, M. J., see Holland, C. K.

Clonogenicity
the combined effects of high-energy shock waves and ionising radiation on a human bladder cancer cell line (Fickweiler), 1097

Cloutier, G., see Allard, L.

Clutter
a Doppler ultrasound clutter phantom (Rickey), 747

Coakley, W. T., see Thomas, N. E.
Cobbold, R. S. C., see Lim, B.

Coeliac axis
comparison of trans- and intra-abdominal duplex examinations of the splanchnic circulation (Delahunt), 165

Coleman, A. J., Choi, M. J. and Saunders, J. E.: detection of acoustic emission from cavitation in tissue during clinical extracorporeal lithotripsy, 1079

Collagen
factors affecting the ultrasonic properties of equine digital flexor tendons (Miles), 907

Collins, W. P., see Tailor, A.

Colour flow
accuracy of color Doppler velocity in the flow field proximal to a regurgitant orifice: implications for color Doppler quantitation of valvular incompetence (Perry), 605
correlation of histomorphology of ovarian masses with color Doppler sonography (Fleischer), 555
direct evidence of cavitation *in vivo* from diagnostic ultrasound (Holland), 917
high resolution 3D color flow mapping: applied to the assessment of breast vasculature (Ferrara), 293
pitfalls in the diagnosis of origin stenosis of the coeliac and superior mesenteric arteries with transabdominal colour duplex examination (Geelkerken), 695
power Doppler: an advance over colour Doppler for transcranial imaging? (Kenton), 313
ultrasonic–pathologic comparison of postangioplasty myointimal hyperplasia and primary atheroma of the superficial femoral artery (Baumgartner), 815
velocity vector reconstruction for color flow Doppler: experimental evaluation of a new geometrical method (Giarré), 75

Colucci, V., see Hynynen, K.

Combination therapy
the combined effects of high-energy shock waves and ionising radiation on a human bladder cancer cell line (Fickweiler), 1097

Compounding
spatial compounding in ultrasonic imaging using an articulated scan arm (Hernandez), 229

Compression
estimating tissue strain from signal decorrelation using the correlation coefficient (Varghese), 1249
imaging of the elastic properties of tissues — a review (Gao), 959
noise reduction in elastograms using temporal stretching with multicompression averaging (Varghese), 1043
particle and voxel approaches for simulating ultrasound backscattering from tissue (Lim), 1237

reduction of stress nonuniformities by apodization of compressor displacement in elastography (Konofagou), 1229

Conant, E. F., see Forsberg, F.

Contractility

influence of preload, afterload and contractility on myocardial ultrasonic tissue characterization with integrated backscatter (Naito), 305

the relationship between myocardial integrated backscatter, perfusion pressure and wall thickness during isovolumic contraction: an isolated pig heart study (Rijsterborgh), 43

Contrast

a review of *in vitro* bioeffects of inertial ultrasonic cavitation from a mechanistic perspective (Miller), 1131

contrast-agent gas bodies enhance hemolysis induced by lithotripter shock waves and high-intensity focused ultrasound in whole blood (Miller), 1089

effects of shadowing on the time–intensity curves in contrast echocardiography: a phantom study (Bos), 217

fundamental limitations on the contrast-transfer efficiency in elastography: an analytic study (Kallel), 463

hemolysis of Albunex-supplemented, 40% hematocrit human erythrocytes *in vitro* by 1-MHz pulsed ultrasound: acoustic pressure and pulse length dependence (Brayman), 927

pharmacokinetic studies of different echo-contrast agents in the cerebral circulation of dogs (Seidel), 1037

quantitative measurements of second harmonic Doppler using ultrasound contrast agents (Chang), 1205

real-time assessment of the parameter of nonlinearity in tissue using "nonlinear shadowing" (Fatemi), 1215

some considerations on the measurements of mean frequency shift and integrated backscatter following administration of Albunex (Wang), 441

temporal correlation of blood scattering signals *in vivo* from radiofrequency intravascular ultrasound (Li), 583

the Doppler kinetics of microbubble echo contrast (Schwarz), 453

Cornel, E. B., see Oosterhof, G. O. N.

Cox, C., see Baggs, R.

Cox, C., see Brayman, A. A.

Cox, C., see Raeman, C. H.

Cox, G. C., see Hall, T. J.

Craven, T., see Riley, W. A.

Cromme-Dijkhuis, A. H., see Djoa, K. K.

Cross-correlation

computation of a location shift between two subsequent intravascular ultrasound registrations by cross-correlation analysis of the lumen area functions (Post), 239

estimating tissue strain from signal decorrelation using the correlation coefficient (Varghese), 1249

temporal correlation of blood scattering signals *in vivo* from radiofrequency intravascular ultrasound (Li), 583

Crosstalk
compensation for phase and amplitude imbalance in quadrature Doppler signals (Moraes), 129

Cryosurgery
interventional ultrasound (Holm), 773

Cullinan, J. A., see Fleischer, A. C.

Cyclic variation
cyclic variation of Doppler power from whole blood under pulsatile flow (Wu), 883

Cyr, D. R., see Ritchie, C. J.

D

D'Arcy, T. J., see Hughes, S. W.
Dalecki, D., Raeman, C. H., Child, S. Z. and Carstensen, E. L.: a test for cavitation as a mechanism for intestinal hemorrhage in mice exposed to a piezoelectric lithotripter, 493
Dalecki, D., see Baggs, R.
Dalecki, D., see Raeman, C. H.
Davies, I. ab. I., see Gavrilov, L. R.
De Jong, N., see Djoa, K. K.
Debruyne, F. M. J., see Oosterhof, G. O. N.
Debus, J., see Jöchle, K.
Delahunt, T. A., Geelkerken, R. H., Hermans, J., van Baalen, J. M., Vaughn, A. J. and van Bockel, J. H.: comparison of trans- and intra-abdominal duplex examinations of the splanchnic circulation, 165
Deng, C. X., see Holland, C. K.
Deng, C. X., Xu, Q., Apfel, R. E. and Holland, C. K.: *in vitro* measurements of inertial cavitation thresholds in human blood, 939
Deng, J., Gardener, J. E., Rodeck, C. H. and Lees, W. R.: fetal echocardiography in three and four dimensions, 979

Densitometry
effects of shadowing on the time–intensity curves in contrast echocardiography: a phantom study (Bos), 217

Derating
finite amplitude distortion and its relationship to linear derating formulae for diagnostic ultrasound systems (Christopher), 1103

Diabetes mellitus
increased stiffness of the aorta in children and adolescents with insulin-dependent diabetes mellitus (Hu), 537

Digital filters
compensation for phase and amplitude imbalance in quadrature Doppler signals (Moraes), 129

Dilatation
new methods for arterial diameter measurement from B-mode images (Stadler), 25

Dissection
residual stenosis determined by intravascular ultrasound and duplex ultrasound after balloon angioplasty of the superficial femoral artery (Pasterkamp), 801

Distortion
finite amplitude distortion and its relationship to linear derating formulae for diagnostic ultrasound systems (Christopher), 1103
quantitative measurements of second harmonic Doppler using ultrasound contrast agents (Chang), 1205
real-time assessment of the parameter of nonlinearity in tissue using "nonlinear shadowing" (Fatemi), 1215

Djoa, K. K., De Jong, N., Cromme-Dijkhuis, A. H., Lancée, C. T. and Bom, N.: two decades of transesophageal phased array probes, 1

DNA
factors affecting the ultrasonic properties of equine digital flexor tendons (Miles), 907
the role of cavitation in the induction of cellular DNA damage by ultrasound and lithotripter shock waves *in vitro* (Miller), 681

Do, D.-D., see Baumgartner, I.
Doi, Y., see Naito, J.
Dong, M.-L., Kofke, W. A., Policare, R. S., Wang, A. S., Acuff, J., Sekhar, L. N. and Jannetta, P. J.: transcranial Doppler ultrasonography in neurosurgery: effects of intracranial tumour on right middle cerebral artery flow velocity during induction of anaesthesia, 1163

Doppler
a comparison of intratumoural indices of blood flow velocity and impedance for the diagnosis of ovarian cancer (Tailor), 837
a Doppler ultrasound clutter phantom (Rickey), 747
a high-frequency continuous-wave Doppler ultrasound system for the detection of blood flow in the microcirculation (Christopher), 1991
accuracy of color Doppler velocity in the flow field proximal to a regurgitant orifice: implications for color Doppler quantitation of valvular incompetence (Perry), 605
an impedance index in normal subjects and in subarachnoid hemorrhage (Giller), 373
assessment of wall velocity gradient imaging using a test phantom (Nowicki), 1255
autocorrelation of integrated power Doppler signals and its application (Chen), 1053
changes in superior mesenteric artery Doppler waveform during reduction of cardiac stroke volume and hypotension (Perko), 11
comparison of Doppler signal analysis techniques for velocity waveform, turbulence and vortex measurement: a simulation study (Wang), 635
comparison of trans- and intra-abdominal duplex examinations of the splanchnic circulation (Delahunt), 165
compensation for phase and amplitude imbalance in quadrature Doppler signals (Moraes), 129 (Technical Note)
computational analysis of the ductus venosus fluid dynamics based on Doppler measurements (Pennati), 1017

correlation of histomorphology of ovarian masses with color Doppler sonography (Fleischer), 555
cyclic variation of Doppler power from whole blood under pulsatile flow (Wu), 883
development of quantitative Doppler indices for uteroplacental and fetal blood flow during the third trimester (Joern), 823
diagnosis and follow-up of carotid-cavernous fistulas by carotid duplex sonography and transcranial color Doppler imaging (Chen), 1155
differentiation between emboli and artefacts using dual-gated transcranial Doppler ultrasound (Smith), 1031
direct evidence of cavitation *in vivo* from diagnostic ultrasound (Holland), 917
downstream determinants of pulsatility of the mean velocity waveform in the umbilical artery as predicted by a computer model (Surat), 707
evaluation of an automated real-time spectral analysis technique (Rickey), 61
evaluation of normal and abnormal hyoid bone movement during swallowing by use of ultrasound duplex-Doppler imaging (Sonies), 1169
hemodynamic assessement of carbomedics bileaflet heart valves by ultrasound: studies in the aortic and mitral positions (Cape), 421
high resolution 3D color flow mapping: applied to the assessment of breast vasculature (Ferrara), 293
nonlinear transcranial Doppler analysis demonstrates age-related changes of cerebral hemodynamics (Keunen), 383
observer variability in volumetric blood flow measurements in leg arteries using duplex ultrasound (Hussain), 287
pharmacokinetic studies of different echo-contrast agents in the cerebral circulation of dogs (Seidel), 1037
pitfalls in the diagnosis of origin stenosis of the coeliac and superior mesenteric arteries with transabdominal colour duplex examination (Geelkerken), 695
power Doppler: an advance over colour Doppler for transcranial imaging? (Kenton), 313
quantitative measurements of second harmonic Doppler using ultrasound contrast agents (Chang), 1205
residual stenosis determined by intravascular ultrasound and duplex ultrasound after balloon angioplasty of the superficial femoral artery (Pasterkamp), 801
simulating nonstationary in-phase and quadrature Doppler signals using a time-varying impulse response filter (Wang), 529 (Letter)
subtraction procedure for the registration of tissue perfusion with Doppler ultrasound (Bührer), 651
the application of echo-tracking methods to endothelium-dependent vasoreactivity and arterial compliance measurements (Stadler), 35
the Doppler kinetics of microbubble echo contrast (Schwarz), 453
the influence of acoustic impedance mismatch on poststenotic pulsed-Doppler ultrasound measurements in a coronary artery model (Jones), 623
three-dimensional power Doppler imaging: a phantom study to quantify vessel stenosis (Guo), 1059
three-dimensional ultrasonic angiography using power-mode Doppler (Ritchie), 277
transcranial Doppler sonography at the early stage of acute central nervous system infections in adults (Müller), 173

transcranial Doppler ultrasonography in neurosurgery: effects of intracranial tumour on right middle cerebral artery flow velocity during induction of anaesthesia (Deng), 1163
ultrasonic–pathologic comparison of postangioplasty myointimal hyperplasia and primary atheroma of the superficial femoral artery (Baumgartner), 815
velocity vector reconstruction for color flow Doppler: experimental evaluation of a new geometrical method (Giarré), 75
verification of cardiac Doppler tissue images using grey-scale M-mode images (Fleming), 573
volumetric flow estimation *in vivo* and *in vitro* using pulsed-Doppler ultrasound (Holland), 591

Doppler tissue imaging
verification of cardiac Doppler tissue images using grey-scale M-mode images (Fleming), 573

Doppler waveform
changes in superior mesenteric artery Doppler waveform during reduction of cardiac stroke volume and hypotension (Perko), 11
comparison of Doppler signal analysis techniques for velocity waveform, turbulence and vortex measurement: a simulation study (Wang), 635
evaluation of an automated real-time spectral analysis technique (Rickey), 61

Doukas, A. G. and Flotte, T. J.: physical characteristics and biological effects of laser-induced stress waves, 151
Doukas, A. G., see Lee, S.
Dousse, B., see Giarré, M.
Downey, D. B., see Tong, S.

Ductus venosus
computational analysis of the ductus venosus fluid dynamics based on Doppler measurements (Pennati), 1017

Dudley, N. J. and Griffith, K.: the importance of rigorous testing of circumference measuring callipers, 1117
van der Dungen, J. J. A. M., see Lijmer, J. G.

Duplex
a high-frequency continuous-wave Doppler ultrasound system for the detection of blood flow in the microcirculation (Christopher), 1991
colour duplex ultrasound assessment of lower limb arterial disease: the effect of adjacent disease (Sensier), 365 (Letter)
comparison of trans- and intra-abdominal duplex examinations of the splanchnic circulation (Delahunt), 165
diagnosis and follow-up of carotid-cavernous fistulas by carotid duplex sonography and transcranial color Doppler imaging (Chen), 1155
evaluation of normal and abnormal hyoid bone movement during swallowing by use of ultrasound duplex-Doppler imaging (Sonies), 1169
in response to Drs. Sensier and London (Allard), 365 (Letter)
observer variability in volumetric blood flow measurements in leg arteries using duplex ultrasound (Hussain), 287

Durand, L.-G., see Allard, L.

Dutta, P., see Konofagou, E.

E

Echocardiography
accuracy of color Doppler velocity in the flow field proximal to a regurgitant orifice: implications for color Doppler quantitation of valvular incompetence (Perry), 605
analysis of transmural trend of myocardial integrated ultrasonic backscatter in patients with old myocardial infarction (Naito), 807
assessment of wall velocity gradient imaging using a test phantom (Nowicki), 1255
effects of shadowing on the time–intensity curves in contrast echocardiography: a phantom study (Bos), 217
fetal echocardiography in three and four dimensions (Deng), 979
hemodynamic assessment of carbomedics bileaflet heart valves by ultrasound: studies in the aortic and mitral positions (Cape), 421
nearly real-time visualization of arbitrary two-dimensional sections from three-dimensional acquisition (Capineri), 319
the Doppler kinetics of microbubble echo contrast (Schwarz), 453
two decades of transesophageal phased array probes (Djoa), 1

Echo tracking
a noninvasive method to estimate arterial impedance by means of assessment of local diameter change and the local center-line blood flow velocity using ultrasound (Brands), 895
the application of echo-tracking methods to endothelium-dependent vasoreactivity and arterial compliance measurements (Stadler), 35

Eder, G., Harkányi, Z. and Schaff, Z.: ultrasound guided spleen biopsy in chimpanzees (pan troglodytes), 19

Edge detection
new methods for arterial diameter measurement from B-mode images (Stadler), 25

Edwards, W. S., see Ritchie, C. J.

Elastic modulus
imaging of the elastic properties of tissues—a review (Gao), 959

Elasticity
estimating tissue strain from signal decorrelation using the correlation coefficient (Varghese), 1249
fundamental limitations on the contrast-transfer efficiency in elastography: an analytic study (Kallel), 463
imaging of the elastic properties of tissues—a review (Gao), 959
noise reduction in elastograms using temporal stretching with multicompression averaging (Varghese), 1043
reduction of stress nonuniformities by apodization of compressor displacement in elastography (Konofagou), 1229

Elastography
estimating tissue strain from signal decorrelation using the correlation coefficient (Varghese), 1249

imaging of the elastic properties of tissues — a review (Gao), 959
noise reduction in elastograms using temporal stretching with multicompression averaging (Varghese), 1043
reduction of stress nonuniformities by apodization of compressor displacement in elastography (Konofagou), 1229

Ell, C., see Feigl, T.

Embolism
differentiation between emboli and artefacts using dual-gated transcranial Doppler ultrasound (Smith), 1031

Encephalitis
transcranial Doppler sonography at the early stage of acute central nervous system infections in adults (Müller), 173

Endarterectomy
differentiation between emboli and artefacts using dual-gated transcranial Doppler ultrasound (Smith), 1031

Endl, E., Steinbach, P., Schärfe, J., Fickweiler, S., Wörle, K. and Hofstädter, F.: cell-type-specific response to shock waves of suspended or pelleted cells as analysed by flow cytometry or electrical cell volume determination, 515

Endothelial-derived relaxing factor
new methods for arterial diameter measurement from B-mode images (Stadler), 25
the application of echo-tracking methods to endothelium-dependent vasoreactivity and arterial compliance measurements (Stadler), 35

Entropy
the distribution of the local entropy in ultrasound images (Zimmer), 431

Equine flexor tendons
factors affecting the ultrasonic properties of equine digital flexor tendons (Miles), 907

Errors
a Doppler ultrasound clutter phantom (Rickey), 747
accuracy of color Doppler velocity in the flow field proximal to a regurgitant orifice: implications for color Doppler quantitation of valvular incompetence (Perry), 605
comparison of Doppler signal analysis techniques for velocity waveform, turbulence and vortex measurement: a simulation study (Wang), 635
comparison of trans- and intra-abdominal duplex examinations of the splanchnic circulation (Delahunt), 165
computation of a location shift between two subsequent intravascular ultrasound registrations by cross-correlation analysis of the lumen area functions (Post), 239
interobserver reproductibility of qualitative and quantitative analysis of intravascular ultrasound images before and after peripheral balloon angioplasty (van der Lugt), 399
observer variability in volumetric blood flow measurements in leg arteries using duplex ultrasound (Hussain), 287

precision and accuracy of acoustospectrographic parameters (Huisman), 855
reproducibility of extracranial carotoid atherosclerotic lesions assessed by B-mode ultrasound: the atherosclerosis risk in communities study (Li), 791
residual stenosis determined by intravascular ultrasound and duplex ultrasound after balloon angioplasty of the superficial femoral artery (Pasterkamp), 801
ROC analysis of noninvasive tests for peripheral arterial disease (Lijmer), 391
the importance of rigorous testing of circumference measuring callipers (Dudley), 1117 (Technical Note)
the influence of acoustic impedance mismatch on poststenotic pulsed-Doppler ultrasound measurements in a coronary artery model (Jones), 623
three-dimensional power Doppler imaging: a phantom study to quantify vessel stenosis (Guo), 1059
variability in B-mode ultrasound measurements in the atherosclerosis risk in communities (ARIC) study (Chambless), 545
volumetric flow estimation *in vivo* and *in vitro* using pulsed-Doppler ultrasound (Holland), 591

Erythrocytes
contrast-agent gas bodies enhance hemolysis induced by lithotripter shock waves and high-intensity focused ultrasound in whole blood (Miller), 1089
hemolysis of Albunex-supplemented, 40% hematocrit human erythrocytes *in vitro* by 1-MHz pulsed ultrasound: acoustic pressure and pulse length dependence (Brayman), 927
in vitro measurements of inertial cavitation thresholds in human blood (Deng), 939

Etani, H., see Yagita, Y.
Etienne, J., see Nowicki, A.
Evans, D. H., see Kenton, A. R.
Evans, D. H., see Moraes, R.
Evans, D. H., see Smith, J. L.

Extravasation
direct evidence of cavitation *in vivo* from diagnostic ultrasound (Holland), 917

F

Fan, L., see Smith, J. L.
Fan, P. H., see Perry, G. J.
Fan, X. and Hynynen, K.: ultrasound surgery using multiple sonications—treatment time considerations, 471

Fat
real-time assessment of the parameter of nonlinearity in tissue using "nonlinear shadowing" (Fatemi), 1215

Fatemi, M. and Greenleaf, J. F.: real-time assessment of the parameter of nonlinearity in tissue using "nonlinear shadowing," 1215
Feigl, T., Völklein, B., Iro, H., Ell, C. and Schneider, T.: biophysical effects of high-energy pulsed ultrasound on human cells, 1267

Femoral artery
ultrasonic–pathologic comparison of postangioplasty myointimal hyperplasia and primary atheroma of the superficial femoral artery (Baumgartner), 815

Fendel, H., see Joern, H.
Fenn, L. N., see Fleming, A. D.
Fenster, A., see Guo, Z.
Fenster, A., see Rickey, D. W.
Fenster, A., see Tong, S.
Fernandez, L. A., see Holland, C. K.
Ferrara, K., Zagar, B., Sokil-Melgar, J. and Algazi, V. R.: high resolution 3D color flow mapping: applied to the assessment of breast vasculature, 293
Ferrazzi, E., see Pennati, G.

Fetus
a test for cavitation as a mechanism for intestinal hemorrhage in mice exposed to a piezoelectric lithotripter (Dalecki), 493
computational analysis of the ductus venosus fluid dynamics based on Doppler measurements (Pennati), 1017
development of quantitative Doppler indices for uteroplacental and fetal blood flow during the third trimester (Joern), 823
downstream determinants of pulsatility of the mean velocity waveform in the umbilical artery as predicted by a computer model (Surat), 707

Fibre
factors affecting the ultrasonic properties of equine digital flexor tendons (Miles), 907

Fickweiler, S., see Endl, E.
Fickweiler, S., Steinbach, P., Wörle, K. and Hofstädter, F.: the combined effects of high-energy shock waves and ionising radiation on a human bladder cancer cell line, 1097
Filipczynski, L., Kujawska, T., Tymkiewicz, R. and Wójcik, J.: amplitude, isobar and grey-scale imaging of ultrasonic shadows behind rigid, elastic and gaseous spheres, 261

Fine needle biopsy
biopsy of nonpalpable cervical lymph nodes: selection criteria for ultrasound-guided biopsy in patients with head and neck squamous cell carcinoma (Kruyt), 413
interventional ultrasound (Holm), 773
ultrasound-guided spleen biopsy in chimpanzees (pan troglodytes) (Eder), 19

Finite amplitude effects
fundamental limitations on the contrast-transfer efficiency in elastography: an analytic study (Kallel), 463

Fish, P. J., see Wang, Y.
Fleischer, A. C., Cullinan, J. A., Jones III, H. W. and Page, D. L.: correlation of histomorphology of ovarian masses with color Doppler sonography, 555

Fleming, A. D., Palka, P., McDicken, W. N., Fenn, L. N. and Sutherland, G. R.: verification of cardiac Doppler tissue images using grey-scale M-mode images, 573
Flotte, T. J., see Doukas, A. G.
Flotte, T. J., see Lee, S.

Flow cytometry
in vitro mechanisms of chemopotentiation by tone-burst ultrasound (Harrison), 355

Flow fields
accuracy of color Doppler velocity in the flow field proximal to a regurgitant orifice: implications for color Doppler quantitation of valvular incompetence (Perry), 605
the influence of acoustic impedance mismatch on poststenotic pulsed-Doppler ultrasound measurements in a coronary artery model (Jones), 623

Focused US
application of focused ultrasound for the stimulation of neural structures (Gavrilov), 179
interventional ultrasound (Holm), 773
potential adverse effects of high-intensity focused ultrasound exposure on blood vessels *in vivo* (Hynynen), 193

Folsom, A. R., see Chambless, L. E.
Forsberg, F., Conant, E. F., Russell, K. M. and Moore, J. H., Jr.: quantitative ultrasonic diagnosis of silicone breast implant rupture: an *in vitro* feasibility study, 53
Forsberg, F., see Shankar, P. M.
Foster, F. S., see Christopher, D. A.
Foster, F. S., see Turnbull, D. H.

Four dimensional
fetal echocardiography in three and four dimensions (Deng), 979

Fowlkes, J. B., see Chen, J.-F.

Fragmentation
physics of ultrasonic surgery using tissue fragmentation: part I (Cimino), 89

Freer, A.: practical sonography in obstetrics and gynaecology (2nd edition), 689 (Book Review)
From, L., see Turnbull, D. H.
Funk, A., see Joern, H.
Furberg, C. D., see Riley, W. A.
Fursey, G. A. J., see Miles, C. A.

G

Gao, L., Parker, K. J., Lerner, R. M. and Levinson, S. F.: imaging of the elastic properties of tissues—a review, 959
Gardener, J. E., see Deng, J.
Gavrilov, L. R., Tsirulnikov, E. M. and Davies, I. ab. I.: application of focused ultrasound for the stimulation of neural structures, 179

Geelkerken, R. H., Delahunt, T. A., Schultze Kool, L. J., van Baalen, J. M. and Hermans, J.: pitfalls in the diagnosis of origin stenosis of the coeliac and superior mesenteric arteries with transabdominal colour duplex examination, 695
Geelkerken, R. H., see Delahunt, T. A.
Genis, V., see Shankar, P. M.
Gennser, G., see Hu, J.
Giarré, M., Dousse, B. and Meister, J.-J.: velocity vector reconstruction for color flow Doppler: experimental evaluation of a new geometrical method, 75
Giller, A., see Giller, C. A.
Giller, C. A., Ratcliff, B., Berger, B. and Giller, A.: an impedance index in normal subjects and in subarachnoid hemorrhage, 373
Gimenez, G., see Hernandez, A.

Glomerular size
ultrasonic measurement of glomerular diameters in normal adult humans (Hall), 987

Glycosaminoglycans
factors affecting the ultrasonic properties of equine digital flexor tendons (Miles), 907

Goetz, M., see Joern, H.
Goldberg, B. B., see Shankar, P. M.
Green, D. W., see Perry, G. J.
Greenleaf, J. F., see Fatemi, M.
Griffith, K., see Dudley, N. J.
de Groot, E., see van Swinjdregt, A. D. M.

Guidance
biopsy of nonpalpable cervical lymph nodes: selection criteria for ultrasound-guided biopsy in patients with head and neck squamous cell carcinoma (Kruyt), 413
interventional ultrasound (Holm), 773
noninvasive arterial occlusion using MRI-guided focused ultrasound (Hynynen), 1071
ultrasound-guided spleen biopsy in chimpanzees (pan troglodytes) (Eder), 19

Guo, Z. and Fenster, A.: three-dimensional power Doppler imaging: a phantom study to quantify vessel stenosis, 1059
Gussenhoven, E. J., see Li, W.
Gussenhoven, E. J., see van Swijndregt, A. D. M.
Gussenhoven, E. J., see van der Lugt, A.
Gutierrez, P. L., see Harrison, G. H.

H

ter Haar, G. R.: the acoustic bubble, 527 (Book Review)
ter Haar, G. R., see Malcolm, A. L.
ter Haar, G. R., see Watkin, N. A.
Hall, T. J., Insana, M. F., Harrison, L. A. and Cox, G. C.: ultrasonic measurement of glomerular diameters in normal adult humans, 987
Handa, N., see Yagita, Y.

Hardness
imaging of the elastic properties of tissues—a review (Gao), 959

Harkányi, Z., see Eder, G.

Harmonic
quantitative measurements of second harmonic Doppler using ultrasound contrast agents (Chang), 1205

Harrison, G. H., Balcer-Kubiczek, E. K. and Gutierrez, P. L.: *in vitro* mechanisms of chemopotentiation by tone-burst ultrasound, 355
Harrison, L. A., see Hall, T. J.

Heart
the relationship between myocardial integrated backscatter, perfusion pressure and wall thickness during isovolumic contraction: an isolated pig heart study (Rijsterborgh),
two decades of transesophageal phased array probes (Djoa), 1

Heating
ablation of tissue volumes using high intensity focused ultrasound (Malcolm), 659
finite amplitude distortion and its relationship to linear derating formulae for diagnostic ultrasound systems (Christopher), 1103
noninvasive arterial occlusion using MRI-guided focused ultrasound (Hynynen), 1071
perfusion corrections for ultrasonic heating in nonperfused media (Shaw), 203
ultrasound surgery using multiple sonications—treatment time considerations (Fan), 471

Heiss, G., see Chambless, L. E.
Heiss, G., see Li, R.

Hemangioma
application of artificial neural networks for the classification of liver lesions by image texture parameters (Sujana), 1177

Hematocrit
hemolysis of Albunex-supplemented, 40% hematocrit human eythrocytes *in vitro* by 1-MHz pulsed ultrasound: acoustic pressure and pulse length dependence (Brayman), 927
re-evaluation of the concept that high cell concentrations "protect" cells *in vitro* from ultrasonically induced lysis (Brayman), 497

Hemodynamics
accuracy of color Doppler velocity in the flow field proximal to a regurgitant orifice: implications for color Doppler quantitation of valvular incompetence (Perry), 605
an impedance index in normal subjects and in subarachnoid hemorrhage (Giller), 373
computational analysis of the ductus venosus fluid dynamics based on Doppler measurements (Pennati), 1017

diagnosis and follow-up of carotid-cavernous fistulas by carotid duplex sonography and transcranial color Doppler imaging (Chen), 1155
hemodynamic assessment and carbomedics bileaflet heart valves by ultrasound: studies in the aortic and mitral positions (Cape), 421
volumetric flow estimation *in vivo* and *in vitro* using pulsed-Doppler ultrasound (Holland), 591

Hemolysis
contrast-agent gas bodies enhance hemolysis induced by lithotripter shock waves and high-intensity focused ultrasound in whole blood (Miller), 1089
hemolysis of Albunex-supplemented, 40% hematocrit human erythrocytes *in vitro* by 1-MHz pulsed ultrasound: acoustic pressure and pulse length dependence (Brayman), 927

Hensen, F. and Länne, T.: in response to Drs. Reneman and Hoeks, 273 (Letter)
Hermans, J., Geelkerken, R. H.
Hermans, J., see Delahunt, T. A.
Hermes, M., see Müller, M.
Hernandez, A., Basset, O., Chirossel, P. and Gimenez, G.: spatial compounding in ultrasonic imaging using an articulated scan arm, 229

HESW
a new method of quantitative cavitation assessment in the field of a lithotripter (Jöchle), 329
a review of *in vitro* bioeffects of inertial ultrasonic cavitation from a mechanistic perspective (Miller), 1131
a test for cavitation as a mechanism for intestinal hemorrhage in mice exposed to a piezoelectric lithotripter (Dalecki), 493
alteration of cell membrane by stress waves *in vitro* (Lee), 1285
biophysical effects of high-energy pulsed ultrasound on human cells (Feigl), 1267
cell-type-specific response to shock waves of suspended or pelleted cells as analysed by flow cytometry or electrical cell volume determination (Endl), 515
contrast-agent gas bodies enhance hemolysis induced by lithotripter shock waves and high-intensity focused ultrasound in whole blood (Miller), 1089
detection of acoustic emssion from cavitation in tissue during clinical extracorporeal lithotripsy (Coleman), 1079
disturbance of cellular calcium homeostasis by *in vitro* application of shock waves (Suhr), 671
physical characteristics and biological effects of laser-induced stress waves (Doukas), 151
the combined effects of high-energy shock waves and ionising radiation on a human bladder cancer cell line (Fickweiler), 1097
the influence of high-energy shock waves on the development of metastases (Oosterhof), 339
the role of cavitation in the induction of cellular DNA damage by ultrasound and lithotripter shock waves *in vitro* (Miller), 681

HIFU
ablation of tissue volumes using high intensity focused ultrasound (Malcolm), 659

contrast-agent gas bodies enhance hemolysis induced by lithotripter shock waves and high-intensity focused ultrasound in whole blood (Miller), 1089
detection of acoustic emission from cavitation in tissue during clinical extracorporeal lithotripsy (Coleman), 1079
interventional ultrasound (Holm), 773
noninvasive arterial occlusion using MRI-guided focused ultrasound (Hynynen), 1071

Histomorphology
an *in vitro* evaluation of the line pattern of the near and far walls of carotid arteries using B-mode ultrasound (van Swijndregt), 1007
correlation of histomorphology of ovarian masses with color Doppler sonography (Fleischer), 555
in vitro validation of intravascular ultrasound imaging after balloon angioplasty of coronary artery stenosis (Peters), 999
noninvasive arterial occlusion using MRI-guided focused ultrasound (Hynynen), 1071

HIV-1
ultrasound-guided spleen biopsy in chimpanzees (pan troglodytes) (Eder), 19

Hoeks, A. P. G., see Brands, P. J.
Hoeks, A. P. G., see Reneman, R. S.
Hofstädter, F., see Endl, E.
Hofstädter, F., see Fickweiler, S.
Holland, C. K., Clancy, M. J., Taylor, K. J. W., Alderman, J. L., Purushothaman, K. and McCauley, T. R.: volumetric flow estimation *in vivo* and *in vitro* using pulsed-Doppler ultrasound, 591
Holland, C. K., Deng, C. X., Apfel, R. E., Alderman, J. L., Fernandez, L. A. and Taylor, K. J. W.: direct evidence of cavitation *in vivo* from diagnostic ultrasound, 917
Holland, C. K., see Deng, C. X.
Holm, H. H. and Skjoldbye, B.: interventional ultrasound, 773
Homan, R. J. F., see Berkhoff, A. P.
Honkoop, J., see Li, W.
Hori, M., see Naito, J.

Horse
factors affecting the ultrasonic properties of equine digital flexor tendons (Miles), 907

Hu, J., Wallensteen, M. and Gennser, G.: increased stiffness of the aorta in children and adolescents with insulin-dependent diabetes mellitus, 537
Huber, P., see Jöchle, K.
Hughes, S. W., D'Arcy, T. J., Maxwell, D. J., Chiu, W., Milner, A., Saunders, J. E. and Sheppard, R. J.: volume estimation from multiplanar 2D ultrasound images using a remote electromagnetic position and orientation sensor, 561
Huisman, H. J. and Thijssen, J. M.: precision and accuracy of acoustospectrographic parameters, 855
Hülser, D. F., see Suhr, D.
Hunink, M. G. M., see Lijmer, J. G.

Hussain, S. T., Smith, R. E., Wood, R. F. M. and Bland, M.: observer variability in volumetric blood flow measurements in leg arteries using duplex ultrasound, 287
Hwang, B.-S., see Chen, Y.-W.

Hydrogen peroxide
the role of cavitation in the induction of cellular DNA damage by ultrasound and lithotripter shock waves *in vitro* (Miller), 681

Hydrophones
comment on "characterization of ultrasonic transducers using a fiberoptic sensor" (Kwiek), 143 (Letter)
in response to Dr. Kwiek et al. (Wu), 144 (Letter)

Hynynen, K., Chung, A. H., Colucci, V. and Jolesz, F. A.: potential adverse effects of high-intensity focused ultrasound exposure on blood vessels *in vivo*, 193
Hynynen, K., Colucci, V., Chung, A. and Jolesz, F.: noninvasive arterial occlusion using MRI-guided focused ultrasound, 1071
Hynynen, K., see Fan, X.

Hyoid bone
evaluation of normal and abnormal hyoid bone movement during swallowing by use of ultrasound duplex-Doppler imaging (Sonies), 1169

Hypovolemia
changes in superior mesenteric artery Doppler waveform during reduction of cardiac stroke volume and hypotension (Perko), 11

I

Image processing
a two-dimensional extension of minimum cross entropy thresholding for the segmentation of ultrasound images (Zimmer), 1183
amplitude, isobar and grey-scale imaging of ultrasonic shadows behind rigid, elastic and gaseous spheres (Filipczynski), 261
application of artificial neural networks for the classification of liver lesions by image texture parameters (Sujana), 1177
imaging of the elastic properties of tissues—a review (Gao), 959
measurement of antigen concentration by an ultrasound-enhanced latex immunoagglutination assay (Thomas), 1277
new methods for arterial diameter measurement from B-mode images (Stadler), 25
simulation of ultrasonic imaging with linear arrays in causal absorptive media (Berkhoff), 245
spatial compounding in ultrasonic imaging using an articulated scan arm (Hernandez), 229
three-dimensional ultrasonic angiography using power-mode Doppler (Ritchie), 277
volume estimation from multiplanar 2D ultrasound images using a remote electromagnetic position and orientation sensor (Hughes), 561

Image quality
simulation of ultrasonic imaging with linear arrays in causal absorptive media (Berkhoff), 245

Imaging
amplitude, isobar and grey-scale imaging of ultrasonic shadows behind rigid, elastic and gaseous spheres (Filipczynski), 261
an *in vitro* evaluation of the line pattern of the near and far walls of carotid arteries using B-mode ultrasound (van Swijndregt), 1007
assessment of wall velocity gradient imaging using a test phantom (Nowicki), 1255
evaluation of normal and abnormal hyoid bone movement during swallowing by use of ultrasound duplex-Doppler imaging (Sonies), 1169
imaging of the elastic properties of tissues—a review (Gao), 959
in vitro validation of intravascular ultrasound imaging after balloon angioplasty of coronary artery stenosis (Peters), 999
noise reduction in elastograms using temporal stretching with multicompression averaging (Varghese), 1043
real-time assessment of the parameter of nonlinearity in tissue using "nonlinear shadowing" (Fatemi), 1215
reduction of stress nonuniformities by apodization of compressor displacement in elastography (Konofagou), 1229
simulation of ultrasonic imaging with linear arrays in causal absorptive media (Berkhoff), 245
three-dimensional power Doppler imaging: a phantom study to quantify vessel stenosis (Guo), 1059
ultrasonic measurement of glomerular diameters in normal adult humans (Hall), 987

Immunometrics
measurement of antigen concentration by an ultrasound-enhanced latex immunoagglutination assay (Thomas), 1277

Impedance index
an impedance index in normal subjects and in subarachnoid hemorrhage (Giller), 373

Imuta, N., see Yagita, Y.

Infarction
analysis of transmural trend of myocardial integrated ultrasonic backscatter in patients with old myocardial infarction (Naito), 807

Inoue, M., see Naito, J.
Insana, M. F., see Hall, T. J.

Integrated backscatter
analysis of transmural trend of myocardial integrated ultrasonic backscatter in patients with old myocardial infarction (Naito), 807
autocorrelation of integrated power Doppler signals and its application (Chen), 1053
cyclic variation of Doppler power from whole blood under pulsatile flow (Wu), 883
factors affecting the ultrasonic properties of equine digital flexor tendons (Miles), 907
influence of preload, afterload and contractility on myocardial ultrasonic tissue characterization with integrated backscatter (Naito), 305

particle and voxel approaches for simulating ultrasound backscattering from tissue (Lim), 1237
precision and accuracy of acoustospectrographic parameters (Huisman), 855
quantitative ultrasonic diagnosis of silicone breast implant rupture: an *in vitro* feasibility study (Forsberg), 53
some considerations on the measurements of mean frequency shift and integrated backscatter following administration of Albunex (Wang), 441
studies on the use of non-Rayleigh statistics for ultrasonic tissue characterization (Shankar), 873
temporal correlation of blood scattering signals *in vivo* from radiofrequency intravascular ultrasound (Li), 583
the distribution of the local entropy in ultrasound images (Zimmer), 431
the relationship between myocardial integrated backscatter, perfusion pressure and wall thickness during isovolumic contraction: an isolated pig heart study (Rijsterborgh), 43
ultrasonic measurement of glomerular diameters in normal adult humans (Hall), 987
ultrasound backscatter microscope analysis of mouse melanoma progression (Turnbull), 845

Interventional ultrasound
biopsy of nonpalpable cervical lymph nodes: selection criteria for ultrasound-guided biopsy in patients with head and neck squamous cell carcinoma (Kruyt), 413
interventional ultrasound (Holm), 773
noninvasive arterial occlusion using MRI-guided focused ultrasound (Hynynen), 1071
ultrasound-guided spleen biopsy in chimpanzees (pan troglodytes) (Eder), 19

Intestinal hemorrhage
a test for cavitation as a mechanism for intestinal hemorrhage in mice exposed to a piezoelectric lithotripter (Dalecki), 493

Intracranial pressure
transcranial Doppler sonography at the early stage of acute central nervous system infections in adults (Müller), 173

Ionizing radiation
the combined effects of high-energy shock waves and ionising radiation on a human bladder cancer cell line (Fickweiler), 1097

Irmer, U., see Suhr, D.
Iro, H., see Feigl, T.

Irradiation
a review of *in vitro* bioeffects of inertial ultrasonic cavitation from a mechanistic perspective (Miller), 1131
ablation of tissue volumes using high intensity focused ultrasound (Malcolm), 659
alteration of cell membrane by stress waves *in vitro* (Lee), 1285
application of focused ultrasound for the stimulation of neural structures (Gavrilov), 179

biophysical effects of high-energy pulsed ultrasound on human cells (Feigl), 1267
cell-type-specific response to shock waves of suspended or pelleted cells as analysed by flow cytometry or electrical cell volume determination (Endl), 515
detection of acoustic emission from cavitation in tissue during clinical extracorporeal lithotripsy (Coleman), 1079
direct evidence of cavitation *in vivo* from diagnostic ultrasound (Holland), 917
disturbance of cellular calcium homeostasis by *in vitro* application of shock waves (Suhr), 671
exposure-time dependence of the threshold for ultrasonically induced murine lung hemorrhage (Raeman), 139
hemolysis of Albunex-supplemented, 40% hematocrit human erythrocytes *in vitro* by 1-MHz pulsed ultrasound: acoustic pressure and pulse length dependence (Brayman), 927
in vitro mechanisms of chemopotentiation by tone-burst ultrasound (Harrison), 355
noninvasive arterial occlusion using MRI-guided focused ultrasound (Hynynen), 1071
physical characteristics and biological effects of laser-induced stress waves (Doukas), 151
physics of ultrasonic surgery using tissue fragmentation: part I (Cimino), 89
physics of ultrasonic surgery using tissue fragmentation: part II (Bond), 101
potential adverse effects of high-intensity focused ultrasound exposure on blood vessels *in vivo* (Hynynen), 193
rabbit and pig lung damage comparison from exposure to continuous wave 30-kHz ultrasound (O'Brien), 345
the influence of high-energy shock waves on the development of metastases (Oosterhof), 339
the intensity dependence of the site of maximal energy deposition in focused ultrasound surgery (Watkin), 483
thresholds for ultrasonically induced lung hemorrhage in neonatal swine (Baggs), 119
ultrasound surgery using multiple sonications — treatment time considerations (Fan), 471

Isolated heart
the relationship between myocardial integrated backscatter, perfusion pressure and wall thickness during isovolumic contraction: an isolated pig heart study (Rijsterborgh), 43

Isovolumic contraction
the relationship between myocardial integrated backscatter, perfusion pressure and wall thickness during isovolumic contraction: an isolated pig heart study (Rijsterborgh), 43

Itoh, T., see Yagita, Y.

J

Jannetta, P. J., see Dong, M.-L.
Jeng, J.-S., see Chen, Y.-W.
Jöchle, K., Debus, J., Lorenz, W. J. and Huber, P.: a new method of quantitative cavitation assessment in the field of a lithotripter, 329

Joern, H., Funk, A., Goetz, M., Kuehlwein, H., Klein, A. and Fendel, H.: development of quantitative Doppler indices for uteroplacental and fetal blood flow during the third trimester, 823
Jolesz, F. A., see Hynynen, K.
Jones III, H. W., see Fleischer, A. C.
Jones, S. A., Leclerc, H., Chatzimavroudis, G. P., Kim, Y. H., Scott, N. A. and Yoganathan, A. P.: the influence of acoustic impedance mismatch on poststenotic pulsed-Doppler ultrasound measurements in a coronary artery model, 623
Jurkovic, D., see Tailor, A.
Just, S., see Perko, M. J.

K

Kallel, F., Bertrand, M. and Ophir, J.: fundamental limitations on the contrast-transfer efficiency in elastography: an analytic study, 463
Kaps, M., see Seidel, G.
Karl, W. C., see Stadler, R. W.
Karlowicz, P., see Nowicki, A.
Kenton, A. R., Martin, P. J. and Evans, D. H.: power Doppler: an advance over colour Doppler for transcranial imaging?, 313
Keunen, R. W. M., Vliegen, J. H. R., Stam, C. J. and Tavy, D. L. J.: nonlinear transcranial Doppler analysis demonstrates age-related changes of cerebral hemodynamics, 383

Kidney
influence of tissue preparation on the high-frequency acoustic properties of normal kidney tissue (Sasaki), 1261
noninvasive arterial occlusion using MRI-guided focused ultrasound (Hynynen), 1071
ultrasonic measurement of glomerular diameters in normal adult humans (Hall), 987

Kim, Y., see Ritchie, C. J.
Kim, Y. H., see Jones, S. A.
Kinoshita, N., see Yagita, Y.
Klein, A., see Joern, H.
Kofke, W. A., see Dong, M.-L.
Kohles, S. S.: minimal dependence of ultrasonic propagation velocity on frequency, 1297 (Letter)
Kok, W. E. M., see Peters, R. J. G.
Kondo, H., see Naito, J.
Konofagou, E., Dutta, P., Ophir, J. and Céspedes, I.: reduction of stress nonuniformities by apodization of compressor displacement in elastography, 1229
Krams, R., see Rijsterborgh, H.
Krarup, K. C.: handbook of echo-Doppler interpretation, 1295 (Book Review)
Kruyt, R. H., van Putton, W. L. J., Levendag, P. C., de Boer, M. F. and Oudkerk, M.: biopsy of nonpalpable cervical lymph nodes: selection criteria for ultrasound-guided biopsy in patients with head and neck squamous cell carcinoma, 413
Kuehlwein, H., see Joern, H.
Kujawska, T., see Filipczynski, L.
Kwiek, P., Mayer, W. G. and Reibold, R.: comment on "characterization of ultrasonic transducers using a fiberoptic sensor," 143 (Letter)

L

Lancée, C. T., see Djoa, K. K.
Lancée, C. T., see Li, W.
Lancée, C. T., see van Swijndregt, A. D. M.
Lancée, C. T., see Rijsterborgh, H.
Länne, T., see Hensen, F.

Laser
alteration of cell membrane by stress waves *in vitro* (Lee), 1285
interventional ultrasound (Holm), 773
physical characteristics and biological effects of laser-induced stress waves (Doukas), 151

Laser-induced stress waves
alteration of cell membrane by stress waves *in vitro* (Lee), 1285
physical characteristics and biological effects of laser-induced stress waves (Doukas), 151

Latex immunoagglutination assay
measurement of antigen concentration by an ultrasound-enhanced latex immunoagglutination assay (Thomas), 1277

Leclerc, H., see Jones, S. A.
Lee, S., Anderson, T., Zhang, H., Flotte, T. J. and Doukas, A. G.: alteration of cell membrane by stress waves *in vitro,* 1285
Lees, R. S., see Stadler, R. W.
Lees, S.: in response to Dr. Kohles, 1299 (Letter)
Lees, W. R., see Deng, J.
Lerner, R. M., see Gao, L.
Levendag, P. C., see Kruyt, R. H.
Levene, H. B., see Chang, P. H.
Levene, H. B., see Wang, S. H.
Levinson, S. F., see Gao, L.
Lewin, P. A., see Wu, Y. Q.
Li, R., Cai, J., Tegeler, C., Sorlie, P., Metcalf, P. A. and Heiss, G.: reproducibility of extracranial carotid atherosclerotic lesions assessed by B-mode ultrasound: the atherosclerosis risk in communities study, 791
Li, W., van der Steen, A. F. W., Lancée, C. T., Honkoop, J., Gussenhoven, E. J. and Bom, N.: temporal correlation of blood scattering signals *in vivo* from radiofrequency intravascular ultrasound, 583
Lijmer, J. G., Hunink, M. G. M., van der Dungen, J. J. A. M., Loonstra, J. and Smit, A. J.: ROC analysis of noninvasive tests for peripheral arterial disease, 391
Lim, B., Bascom, P. A. J. and Cobbold, R. S. C., particle and voxel approaches for simulating ultrasound backscattering from tissue, 1237

Limb blood flow
observer variability in volumetric blood flow measurements in leg arteries using duplex ultrasound (Hussain), 287

Lin, W.-H., see Chen, Y.-W.
Lindenmayer, A. E., see Shankar, P. M.

Lithotripter
a new method of quantitative cavitation assessment in the field of a lithotripter (Jöchle), 329
a review of *in vitro* bioeffects of inertial ultrasonic cavitation from a mechanistic perspective (Miller), 1131
a test for cavitation as a mechanism for intestinal hemorrhage in mice exposed to a piezoelectric lithotripter (Dalecki), 493
alteration of cell membrane by stress waves *in vitro* (Lee), 1285
biophysical effects of high-energy pulsed ultrasound on human cells (Feigl), 1267
cell-type-specific response to shock waves of suspended or pelleted cells as analysed by flow cytometry or electrical cell volume determination (Endl), 515
contrast-agent gas bodies enhance hemolysis induced by lithotripter shock waves and high-intensity focused ultrasound in whole blood (Miller), 1089
detection of acoustic emission from cavitation in tissue during clinical extracorporeal lithotripsy (Coleman), 1079
disturbance of cellular calcium homeostasis by *in vitro* application of shock waves (Suhr), 671
physical characteristics and biological effects of laser-induced stress waves (Doukas), 151
the combined effects of high-energy shock waves and ionising radiation on a human bladder cancer cell line (Fickweiler), 1097
the influence of high-energy shock waves on the development of metastases (Oosterhof), 339
the role of cavitation in the induction of cellular DNA damage by ultrasound and lithotripter shock waves *in vitro* (Miller), 681

Liu, H.-M., see Chen, Y.-W.

Liver
application of artificial neural networks for the classification of liver lesions by image texture parameters (Sujana), 1177
precision and accuracy of acoustospectrographic parameters (Huisman), 855

London, N. J. M., see Sensier, Y. J.
Loonstra, J., see Lijmer, J. G.
Lorenz, W. J., see Jöchle, K.
van der Lugt, A., Gussenhoven, E. J., Pasterkamp, G., Bom, N., Posthuma, D. J. and Stijnen, T.: interobserver reproducibility of qualitative and quantitative analysis of intravascular ultrasound images before and after peripheral balloon angioplasty, 399

Lung hemorrhage
direct evidence of cavitation *in vivo* from diagnostic ultrasound (Holland), 917
exposure-time dependence of the threshold for ultrasonically induced murine lung hemorrhage (Raeman), 139
rabbit and pig lung damage comparison from exposure to continuous wave 30-kHz ultrasound (O'Brien), 345
thresholds for ultrasonically induced lung hemorrhage in neonatal swine (Baggs), 119

Lymph nodes
biopsy of nonpalpable cervical lymph nodes: selection criteria for ultrasound-guided biopsy in patients with head and neck squamous cell carcinoma (Kruyt), 413

Lymphoid tissue
ultrasound-guided spleen biopsy in chimpanzees (pan troglodytes) (Eder), 19

M

M-mode
verification of cardiac Doppler tissue images using grey-scale M-mode images (Fleming), 573

Mack, L. A., see Ritchie, C. J.
Mahler, F., see Baumgartner, I.
Malcolm, A. L. and ter Haar, G. R.: ablation of tissue volumes using high intensity focused ultrasound, 659
Mali, W. P. T. M., see Pasterkamp, G.
Mali, W. P. T. M., see Post, M. J.
Mano, T., see Naito, J.
Martin, P. J., see Kenton, A. R.
Masotti, L., see Capineri, L.
Mastik, F., see Rijsterborgh, H.
Masuyama, T., see Naito, J.
Matsumoto, M., see Yagita, Y.
Maxwell, D. J., see Hughes, S. W.
Mayer, W. G., see Kwiek, P.
McCauley, T. R., see Holland, C. K.
McDicken, W. N., see Fleming, A. D.

Mechanical index
hemolysis of Albunex-supplemented, 40% hematocrit human erythrocytes *in vitro* by 1-MHz pulsed ultrasound: acoustic pressure and pulse length dependence (Brayman), 927
in vitro measurements of inertial cavitation thresholds in human blood (Deng), 939

Meister, J.-J., see Giarré, M.

Melanoma
ultrasound backscatter microscope analysis of mouse melanoma progression (Turnbull), 845

Membrane permeability
a review of *in vitro* bioeffects of inertial ultrasonic cavitation from a mechanistic perspective (Miller), 1131
alteration of cell membrane by stress waves *in vitro* (Lee), 1285
biophysical effects of high-energy pulsed ultrasound on human cells (Feigl), 1267
cell-type-specific response to shock waves of suspended or pelleted cells as analysed by flow cytometry or electrical cell volume determination (Endl), 515

physical characteristics and biological effects of laser-induced stress waves (Doukas), 151

Meningitis
transcranial Doppler sonography at the early stage of acute central nervous system infections in adults (Müller), 173

Merkelbach, S., see Müller, M.

Metastases
biopsy of nonpalpable cervical lymph nodes: selection criteria for ultrasound-guided biopsy in patients with head and neck squamous cell carcinoma (Kruyt), 413
the influence of high-energy shock waves on the development of metastases (Oosterhof), 339

Metcalf, P. A., see Li, R.

Microbubbles
effects of shadowing on the time–intensity curves in contrast echocardiography: a phantom study (Bos), 217
hemolysis of Albunex-supplemented, 40% hematocrit human erythrocytes *in vitro* by 1-MHz pulsed ultrasound: acoustic pressure and pulse length dependence (Brayman), 927
some considerations on the measurements of mean frequency shift and integrated backscatter following administration of Albunex (Wang), 441
the Doppler kinetics of microbubble echo contrast (Schwarz), 453

Microcirculation
a high-frequency continuous-wave Doppler ultrasound system for the detection of blood flow in the microcirculation (Christopher), 1991
subtraction procedure for the registration of tissue perfusion with Doppler ultrasound (Bührer), 651

Microscope
influence of tissue preparation on the high-frequency acoustic properties of normal kidney tissue (Sasaki), 1261
ultrasound backscatter microscope analysis of mouse melanoma progression (Turnbull), 845

Microwaves
interventional ultrasound (Holm), 773

Miles, C. A., Fursey, G. A. J., Birch, H. L. and Young, R. D.: factors affecting the ultrasonic properties of equine digital flexor tendons, 907
Miller, D. L. and Thomas, R. M.: contrast-agent gas bodies enhance hemolysis induced by lithotripter shock waves and high-intensity focused ultrasound in whole blood, 1089
Miller, D. L. and Thomas, R. M.: the role of cavitation in the induction of cellular DNA damage by ultrasound and lithotripter shock waves *in vitro*, 681
Miller, D. L., see Miller, M. W.
Miller, M. W., Miller, D. L. and Brayman, A. A.: a review of *in vitro* bioeffects of inertial ultrasonic cavitation from a mechanistic perspective, 1131
Miller, M. W., see Brayman, A. A.
Milner, A., see Hughes, S. W.

Minimally invasive surgery
noninvasive arterial occlusion using MRI-guided focused ultrasound (Hynynen), 1071
potential adverse effects of high-intensity focused ultrasound exposure on blood vessels *in vivo* (Hynynen), 193

Minimum cross entropy
a two-dimensional extension of minimum cross entropy thresholding for the segmentation of ultrasound images (Zimmer), 1183

Mitochondria
disturbance of cellular calcium homeostasis by *in vitro* application of shock waves (Suhr), 671

Modelling
a review of *in vitro* bioeffects of inertial ultrasonic cavitation from a mechanistic perspective (Miller), 1131
accuracy of color Doppler velocity in the flow field proximal to a regurgitant orifice: implications for color Doppler quantitation of valvular incompetence (Perry), 605
comparison of Doppler signal analysis: techniques for velocity waveform, turbulence and vortex measurement: a simulation study (Wang), 635
computational analysis of the ductus venosus fluid dynamics based on Doppler measurements (Pennati), 1017
downstream determinants of pulsatility of the mean velocity waveform in the umbilical artery as predicted by a computer model (Surat), 707
fundamental limitations on the contrast-transfer efficiency in elastography: an analytic study (Kallel), 463
particle and voxel approaches for simulating ultrasound backscattering from tissue (Lim), 1237
reduction of stress nonuniformities by apodization of compressor displacement in elastography (Konofagou), 1229
simulation of ultrasonic imaging with linear arrays in causal absorptive media (Berkhoff), 245
the distribution of the local entropy in ultrasound images (Zimmer), 431
the effect of variations in transducer position and sound speed in intravascular ultrasound: a theoretical study (Thompson), 719
the influence of acoustic impedance mismatch on poststenotic pulsed-Doppler ultrasound measurements in a coronary artery model (Jones), 623
two decades of transesophageal phased array probes (Djoa), 1
volumetric flow estimation *in vivo* and *in vitro* using pulsed-Doppler ultrasound (Holland), 591

Molthen, R., see Shankar, P. M.
Moore, J. H., Jr., see Forsberg, F.
Moraes, R. and Evans, D. H.: compensation for phase and amplitude imbalance in quadrature Doppler signals, 129
Moser, U. T., see Bührer, A.

Mouse
a test for cavitation as a mechanism for intestinal hemorrhage in mice exposed to a piezoelectric lithotripter (Dalecki), 493

alteration of cell membrane by stress waves *in vitro* (Lee), 1285
exposure-time dependence of the threshold for ultrasonically induced murine lung hemorrhage (Raeman), 139
rabbit and pig lung damage comparison from exposure to continuous wave 30-kHz ultrasound (O'Brien), 345
ultrasound backscatter microscope analysis of mouse melanoma progression (Turnbull), 845

MRI guidance
noninvasive arterial occlusion using MRI-guided focused ultrasound (Hynynen), 1071

Müller, M., Merkelbach, S., Hermes, M. and Schimrigk, K.: transcranial Doppler sonography at the early stage of acute central nervous system infections in adults, 173

Multicellular tumour spheroids
the combined effects of high-energy shock waves and ionising radiation on a human bladder cancer cell line (Fickweiler), 1097

Multicompression averaging
noise reduction in elastograms using temporal stretching with multicompression averaging (Varghese), 1043

Multiplanar image registration
volume estimation from multiplanar 2D ultrasound images using a remote electromagnetic position and orientation sensor (Hughes), 561

Myocardium
analysis of transmural trend of myocardial integrated ultrasonic backscatter in patients with old myocardial infarction (Naito), 807
effects of shadowing on the time–intensity curves in contrast echocardiography: a phantom study (Bos), 217
influence of preload, afterload and contractility on myocardial ultrasonic tissue characterization with integrated backscatter (Naito), 305
the relationship between myocardial integrated backscatter, perfusion pressure and wall thickness during isovolumic contraction: an isolated pig heart study (Rijsterborgh), 43
verification of cardiac Doppler tissue images using grey-scale M-mode images (Fleming), 573

N

Nagano, R., see Naito, J.
Naito, J., Masuyama, T., Mano, T., Kondo, H., Yamamoto, K., Nagano, R., Inoue, M. and Hori, M.: analysis of transmural trend of myocardial integrated ultrasonic backscatter in patients with old myocardial infarction, 807
Naito, J., Masuyama, T., Mano, T., Yamamoto, K., Doi, Y., Kondo, H., Nagano, R., Inoue, M. and Hori, M.: influence of preload, afterload and contractility on myocardial ultrasonic tissue characterization with integrated backscatter, 305
Nanda, N. C., see Perry, G. J.
Narayanan, V. M., see Shankar, P. M.
Natucci, M., see Tailor, A.
Naylor, A. R., see Smith, J. L.

Neonatal swine
thresholds for ultrasonically induced lung hemorrhage in neonatal swine (Baggs), 119

Neural networks
application of artificial neural networks for the classification of liver lesions by image texture parameters (Sujana), 1177

Neural structures
application of focused ultrasound for the stimulation of neural structures (Gavrilov), 179

Nitta, S.-I., see Sasaki, H.

Nonlinearity
finite amplitude distortion and its relationship to linear derating formulae for diagnostic ultrasound systems (Christopher), 1103
quantitative measurements of second harmonic Doppler using ultrasound contrast agents (Chang), 1205
real-time assessment of the parameter of nonlinearity in tissue using "nonlinear shadowing" (Fatemi), 1215

Nowicki, A., Olszewski, R., Etienne, J., Karlowicz, P. and Adamus, J.: assessment of wall velocity gradient imaging using a test phantom, 1255
Nukada, T., see Yagita, Y.

O

O'Brien, W. D., Jr. and Zachary, J. F.: rabbit and pig lung damage comparison from exposure to continuous wave 30-kHz ultrasound, 345

Observer variability
interobserver reproducibility of qualitative and quantitative analysis of intravascular ultrasound images before and after peripheral balloon angioplasty (van der Lugt), 399
observer variability in volumetric blood flow measurements in leg arteries using duplex ultrasound (Hussain), 287
ROC analysis of noninvasive tests for peripheral arterial disease (Lijmer), 391

Okamoto, M., see Yagita, Y.
Okawai, H., see Sasaki, H.
Olszewski, R., see Nowicki, A.
Oosterhof, G. O. N., Cornel, E. B., Smits, G. A. H. J., Debruyne, F. M. J. and Schalken, J. A.: the influence of high-energy shock waves on the development of metastases, 339
Ophir, J., see Kallel, F.
Ophir, J., see Konofagou, E.
Ophir, J., see Varghese, T.

Optical breakdown
physical characteristics and biological effects of laser-induced stress waves (Doukas), 151

Oudkerk, M., see Kruyt, R. H.

Ovarian cancer
a comparison of intratumoural indices of blood flow velocity and impedance for the diagnosis of ovarian cancer (Tailor), 837

Ovarian cysts
the distribution of the local entropy in ultrasound images (Zimmer), 431

Ovarian masses
a comparison of intratumoural indices of blood flow velocity and impedance for the diagnosis of ovarian cancer (Tailor), 837
correlation of histomorphology of ovarian masses with color Doppler sonography (Fleischer), 555
the distribution of the local entropy in ultrasound images (Zimmer), 431

P

Page, D. L., see Fleischer, A. C.
Palka, P., see Fleming, A. D.
Parker, K. J., see Gao, L.
Pasch, T., see Bührer, A.
Pasterkamp, G., see Post, M. J.
Pasterkamp, G., see van der Lugt, A.
Pasterkamp, G., Spijkerboer, A. M., Mali, W. P. T. M. and Borst, C.: residual stenosis determined by intravascular ultrasound and duplex ultrasound after balloon angioplasty of the superficial femoral artery, 801
Pennati, G., Redaelli, A., Bellotti, M. and Ferrazzi, E.: computational analysis of the ductus venosus fluid dynamics based on Doppler measurements, 1017
Penney, D. P., see Baggs, R.

Perfusion
effects of shadowing on the time–intensity curves in contrast echocardiography: a phantom study (Bos), 217
observer variability in volumetric blood flow measurements in leg arteries using duplex ultrasound (Hussain), 287
perfusion corrections for ultrasonic heating in nonperfused media (Shaw), 203
some considerations on the measurements of mean frequency shift and integrated backscatter following administration of Albunex (Wang), 441
subtraction procedure for the registration of tissue perfusion with Doppler ultrasound (Bührer), 651
the relationship between myocardial integrated backscatter, perfusion pressure and wall thickness during isovolumic contraction: an isolated pig heart study (Rijsterborgh), 43
three-dimensional ultrasonic angiography using power-mode Doppler (Ritchie), 277

Perko, G., see Perko, M. J.
Perko, M. J., Perko, G., Just, S., Secher, N. H. and Schroeder, T. V.: changes in superior mesenteric artery Doppler waveform during reduction of cardiac stroke volume and hypotension, 11
Perry, G. J., Anayiotos, A. S., Green, D. W., Fan, P. H. and Nanda, N. C.: accuracy of color Doppler velocity in the flow field proximal to a regurgitant orifice: implications for color Doppler quantitation of valvular incompetence, 605

Peters, R. J. G., Kok, W. E. M., van der Wal, A. C. and Visser, C. A.: *in vitro* validation of intravascular ultrasound imaging after balloon angioplasty of coronary artery stenosis, 999

Phacoemulsification
physics of ultrasonic surgery using tissue fragmentation: part II (Bond), 101

Phantoms
a Doppler ultrasound clutter phantom (Rickey), 747
accuracy of color Doppler velocity in the flow field proximal to a regurgitant orifice: implications for color Doppler quantitation of valvular incompetence (Perry), 605
assessment of wall velocity gradient imaging using a test phantom (Nowicki), 1255
cyclic variation of Doppler power from whole blood under pulsatile flow (Wu), 883
effects of shadowing on the time–intensity curves in contrast echocardiography: a phantom study (Bos), 217
hemodynamic assessment of carbomedics bileaflet heart valves by ultrasound: studies in the aortic and mitral positions (Cape), 421
high resolution 3D color flow mapping: applied to the assessment of breast vasculature (Ferrara), 293
nearly real-time visualization of arbitrary two-dimensional sections from three-dimensional acquisition (Capineri), 319
perfusion corrections for ultrasonic heating in nonperfused media (Shaw), 203
quantitative measurements of second harmonic Doppler using ultrasound contrast agents (Chang), 1205
real-time assessment of the parameter of nonlinearity in tissue using "nonlinear shadowing" (Fatemi), 1215
subtraction procedure for the registration of tissue perfusion with Doppler ultrasound (Bührer), 651
temporal correlation of blood scattering signals *in vivo* from radiofrequency intravascular ultrasound (Li), 583
the influence of acoustic impedance mismatch on poststenotic pulsed-Doppler ultrasound measurements in a coronary artery model (Jones), 623
three-dimensional power Doppler imaging: a phantom study to quantify vessel stenosis (Guo), 1059
three-dimensional ultrasonic angiography using power-mode Doppler (Ritchie), 277
volumetric flow estimation *in vivo* and *in vitro* using pulsed-Doppler ultrasound (Holland), 591

Phase shifter
compensation for phase and amplitude imbalance in quadrature Doppler signals (Moraes), 129 (Technical Note)

Phased array
two decades of transesophageal phased array probes (Djoa), 1
ultrasound surgery using multiple sonications — treatment time considerations (Fan), 471

Phillips, D., see Schwarz, K. Q.

Photoacoustics
alteration of cell membrane by stress waves *in vitro* (Lee), 1285

PI
a comparison of intratumoural indices of blood flow velocity and impedance for the diagnosis of ovarian cancer (Tailor), 837
changes in superior mesenteric artery Doppler waveform during reduction of cardiac stroke volume and hypotension (Perko), 11
downstream determinants of pulsatility of the mean velocity waveform in the umbilical artery as predicted by a computer model (Surat), 707
evaluation of an automated real-time spectral analysis technique (Rickey), 61
ROC analysis of noninvasive tests for peripheral arterial disease (Lijmer), 391

Piccoli, C. W., see Shankar, P. M.
Piek, J. J., see Bos, L. J.

Pig
rabbit and pig lung damage comparison from exposure to continuous wave 30-kHz ultrasound (O'Brien), 345
temporal correlation of blood scattering signals *in vivo* from radiofrequency intravascular ultrasound (Li), 583
thresholds for ultrasonically induced lung hemorrhage in neonatal swine (Baggs), 119
volumetric flow estimation *in vivo* and *in vitro* using pulsed-Doppler ultrasound (Holland), 591

Pilling, D. W.: a colour atlas of Doppler ultrasonography in obstetrics, 363 (Book Review)

Placenta
development of quantitative Doppler indices for uteroplacental and fetal blood flow during the third trimester (Joern), 823
downstream determinants of pulsatility of the mean velocity waveform in the umbilical artery as predicted by a computer model (Surat), 707

Plaque
in vitro validation of intravascular ultrasound imaging after balloon angioplasty of coronary artery stenosis (Peters), 999
reproducibility of extracranial carotid atherosclerotic lesions assessed by B-mode ultrasound: the atherosclerosis risk in communities study (Li), 791

Policare, R. S., see Dong, M.-L.

Polymerase chain reaction
ultrasound-guided spleen biopsy in chimpanzees (pan troglodytes) (Eder), 19

Post, M. J., Pasterkamp, G., Mali, W. P. T. M. and Borst, C.: computation of a location shift between two subsequent intravascular ultrasound registrations by cross-correlation analysis of the lumen area functions, 239
Posthuma, D. J., see van der Lugt, A.

Power Doppler
autocorrelation of integrated power Doppler signals and its application (Chen), 1053
cyclic variation of Doppler power from whole blood under pulsatile flow (Wu), 883
power Doppler: an advance over colour Doppler for transcranial imaging? (Kenton), 313
three-dimensional power Doppler imaging: a phantom study to quantify vessel stenosis (Guo), 1059
three-dimensional ultrasonic angiography using power-mode Doppler (Ritchie), 277

Pressure drop
computational analysis of the ductus venosus fluid dynamics based on Doppler measurements (Pennati), 1017
hemodynamic assessment of carbomedics bileaflet heart valves by ultrasound: studies in the aortic and mitral positions (Cape), 421

Preston, R. C., see Shaw, A.

Prostate
a three-dimensional ultrasound prostrate imaging system (Tong), 735

Prostheses
hemodynamic assessment of carbomedics bileaflet heart valves by ultrasound: studies in the aortic and mitral positions (Cape), 421
quantitative ultrasonic diagnosis of silicone breast implant rupture: an *in vitro* feasibility study (Forsberg), 53

Proviral DNA
ultrasound-guided spleen biopsy in chimpanzees (pan troglodytes) (Eder), 19

Purushothaman, K., see Holland, C. K.
van Putton, W. L. J., see Kruyt, R. H.

Q

QA
a Doppler ultrasound clutter phantom (Rickey), 747
the importance of rigorous testing of circumference measuring callipers (Dudley), 1117 (Technical Note)

Quadrature phase detection
compensation for phase and amplitude imbalance in quadrature Doppler signals (Moraes), 129

R

Rabbit
rabbit and pig lung damage comparison from exposure to continuous wave 30-kHz ultrasound (O'Brien), 345

Raeman, C. H., Child, S. Z., Dalecki, D., Cox, C. and Carstensen, E. L.: exposure-time dependence of the threshold for ultrasonically induced murine lung hemorrhage, 139

Raeman, C. H., see Baggs, R.
Raeman, C. H., see Dalecki, D.
Ramsay, J. A., see Turnbull, D. H.

Rat
direct evidence of cavitation *in vivo* from diagnostic ultrasound (Holland), 917
the influence of high-energy shock waves on the development of metastases (Oosterhof), 339

Ratcliff, B., see Giller, C. A.

Reciprocity
reduction of stress nonuniformities by apodization of compressor displacement in elastography (Konofagou), 1229

Reconstruction
a three-dimensional ultrasound prostate imaging system (Tong), 735
nearly real-time visualization of arbitrary two-dimensional sections from three-dimensional acquisition (Capineri), 319
spatial compounding in ultrasonic imaging using an articulated scan arm (Hernandez), 229

Redaelli, A., see Pennati, G.
Redha, F., see Baumgartner, I.

Refraction
the effect of variations in transducer position and sound speed in intravascular ultrasound: a theoretical study (Thompson), 719

Registration
spatial compounding in ultrasonic imaging using an articulated scan arm (Hernandez), 229
volume estimation from multiplanar 2D ultrasound images using a remote electromagnetic position and orientation sensor (Hughes), 561

Reibold, R., see Kwiek, P.
Reid, J. M., see Shankar, P. M.

Renal cortex
ultrasonic measurement of glomerular diameters in normal adult humans (Hall), 987

Reneman, R. S. and Hoeks, A. P. G.: diameter and compliance in the human carotid artery — variations with age and sex, 271 (Letter)
Reneman, R. S., see Brands, P. J.

Reproducibility
interobserver reproducibility of qualitative and quantitative analysis of intravascular ultrasound images before and after peripheral balloon angioplasty (van der Lugt), 399
observer variability in volumetric blood flow measurements in leg arteries using duplex ultrasound (Hussain), 287
ROC analysis of noninvasive tests for peripheral arterial disease (Lijmer), 391

reproducibility of extracranial carotid atherosclerotic lesions assessed by B-mode ultrasound: the atherosclerosis risk in communities study (Li), 791
variability in B-mode ultrasound measurements in the atherosclerosis risk in communities (ARIC) study (Chambless), 545

Residual stenosis
residual stenosis determined by intravascular ultrasound and duplex ultrasound after balloon angioplasty of the superficial femoral artery (Pasterkamp), 801
ultrasonic–pathologic comparison of postangioplasty myointimal hyperplasia and primary atheroma of the superficial femoral artery (Baumgartner), 815

Resolution
spatial compounding in ultrasonic imaging using an articulated scan arm (Hernandez), 229
two decades of transesophageal phased array probes (Djoa), 1

Restenosis
ultrasonic–pathologic comparison of postangioplasty myointimal hyperplasia and primary atheroma of the superficial femoral artery (Baumgartner), 815

RF processing
a noninvasive method to estimate arterial impedance by means of assessment of local diameter change and the local center-line blood flow velocity using ultrasound (Brands), 895
analysis of transmural trend of myocardial integrated ultrasonic backscatter in patients with old myocardial infarction (Naito), 807
imaging of the elastic properties of tissues — a review (Gao), 959
influence of preload, afterload and contractility on myocardial ultrasonic tissue characterization with integrated backscatter (Naito), 305
particle and voxel approaches for simulating ultrasound backscattering from tissue (Lim), 1237
temporal correlation of blood scattering signals *in vivo* from radiofrequency intravascular ultrasound (Li), 583
the application of echo-tracking methods to endothelium-dependent vasoreactivity and arterial compliance measurements (Stadler), 35
ultrasonic measurement of glomerular diameters in normal adult humans (Hall), 987

RI
a comparison of intratumoural indices of blood flow velocity and impedance for the diagnosis of ovarian cancer (Tailor), 837
changes in superior mesenteric artery Doppler waveform during reduction of cardiac stroke volume and hypotension (Perko), 11
evaluation of an automated real-time spectral analysis technique (Rickey), 61

Rickey, D. W. and Fenster, A.: a Doppler ultrasound clutter phantom, 747
Rickey, D. W. and Fenster, A.: evaluation of an automated real-time spectral analysis technique, 61
Rijsterborgh, H., see van Swijndregt, A. D. M.

Rijsterborgh, H., van der Steen, A. F. W., Krams, R., Mastik, F., Lancée, C. T., Verdouw, P. D., Roelandt, J. R. T. C. and Bom, N.: the relationship between myocardial integrated backscatter, perfusion pressure and wall thickness during isovolumic contraction: an isolated pig heart study, 43
Riley, W. A., Craven, T., Romont, A. and Furberg, C. D.: assessment of temporal bias in longitudinal measurements of carotid intimal-medial thickness in the asymptomatic carotid artery progression study (ACAPS), 405
Riley, W. A., see Chambless, L. E.
Ritchie, C. J., Edwards, W. S., Mack, L. A., Cyr, D. R. and Kim, Y.: three-dimensional ultrasonic angiography using power-mode Doppler, 277
Rivens, I., see Watkin, N. A.

ROC
quantitative ultrasonic diagnosis of silicone breast implant rupture: an *in vitro* feasibility study (Forsberg), 53
ROC analysis of noninvasive tests for peripheral arterial disease (Lijmer), 391

Rocchi, S., see Capineri, L.
Rodeck, C. H., see Deng, J.
Roelandt, J. R. T. C., see Rijsterborgh, H.
Romont, A., see Riley, W. A.
Rubin, J. M., see Chen, J.-F.
Russell, K. M., see Forsberg, F.
Rutten, M. C. M., see Brands, P. J.

S

S/D
evaluation of an automated real-time spectral analysis technique (Rickey), 61

Safety
biophysical effects of high-energy pulsed ultrasound on human cells (Feigl), 1267
contrast-agent gas bodies enhance hemolysis induced by lithotripter shock waves and high-intensity focused ultrasound in whole blood (Miller), 1089
direct evidence of cavitation *in vivo* from diagnostic ultrasound (Holland), 917
exposure-time dependence of the threshold for ultrasonically induced murine lung hemorrhage (Raeman), 139
finite amplitude distortion and its relationship to linear derating formulae for diagnostic ultrasound systems (Christopher), 1103
hemolysis of Albunex-supplemented, 40% hematocrit human erythrocytes *in vitro* by 1-MHz pulsed ultrasound: acoustic pressure and pulse length dependence (Brayman), 927
potential adverse effects of high-intensity focused ultrasound exposure on blood vessels *in vivo* (Hynynen), 193
rabbit and pig lung damage comparison from exposure to continuous wave 30-kHz ultrasound (O'Brien), 345
thresholds for ultrasonically induced lung hemorrhage in neonatal swine (Baggs), 119

Saijo, Y., see Sasaki, H.

Sapper, D. J., see Sonies, B. C.
Sasaki, H., Saijo, Y., Tanaka, M., Okawai, H., Terasawa, Y., Yambe, T. and Nitta, S.-I.: influence of tissue preparation on the high-frequency acoustic properties of normal kidney tissue, 1261
Sauder, D. N., see Turnbull, D. H.
Saunders, J. E., see Coleman, A. J.
Saunders, J. E., see Hughes, S. W.

Scatter
analysis of transmural trend of myocardial integrated ultrasonic backscatter in patients with old myocardial infarction (Naito), 807
autocorrelation of integrated power Doppler signals and its application (Chen), 1053
cyclic variation of Doppler power from whole blood under pulsatile flow (Wu), 883
factors affecting the ultrasonic properties of equine digital flexor tendons (Miles), 907
influence of preload, afterload and contractility on myocardial ultrasonic tissue characterization with integrated backscatter (Naito), 305
particle and voxel approaches for simulating ultrasound backscattering from tissue (Lim), 1237
precision and accuracy of acoustospectrographic parameters (Huisman), 855
quantitative ultrasonic diagnosis of silicone breast implant rupture: an *in vitro* feasibility study (Forsberg), 53
some considerations on the measurements of mean frequency shift and integrated backscatter following administration of Albunex (Wang), 441
studies on the use of non-Rayleigh statistics for ultrasonic tissue characterization (Shankar), 873
temporal correlation of blood scattering signals *in vivo* from radiofrequency intravascular ultrasound (Li), 583
the distribution of the local entropy in ultrasound images (Zimmer), 431
the relationship between myocardial integrated backscatter, perfusion pressure and wall thickness during isovolumic contraction: an isolated pig heart study (Rijsterborgh), 43
ultrasonic measurement of glomerular diameters in normal adult humans (Hall), 987
ultrasound backscatter microscope analysis of mouse melanoma progression (Turnbull), 845

Schaff, Z., see Eder, G.
Schalken, J. A., see Oosterhof, G. O. N.
Schärfe, J., see Endl, E.
Schimrigk, K., see Müller, M.
Schlief, R., see Schwarz, K. Q.
Schneider, T., see Feigl, T.
Schroeder, T. V., see Perko, M. J.
Schultze Kool, L. J., see Geelkerken, R. H.
Schumacher, P. M., see Bührer, A.
Schwarz, K. Q., Chen, X., Bezante, G. P., Phillips, D. and Schlief, R.: the Doppler kinetics of microbubble echo contrast, 453
Scott, N. A., see Jones, S. A.
Secher, N. H., see Perko, M. J.

Second harmonic
quantitative measurements of second harmonic Doppler using ultrasound contrast agents (Chang), 1205

Segmentation
a two-dimensional extension of minimum cross entropy thresholding for the segmentation of ultrasound images (Zimmer), 1183
fetal echocardiography in three and four dimensions (Deng), 979
the distribution of the local entropy in ultrasound images (Zimmer), 431

Seidel, G., Beller, K.-D. and Kaps, M.: pharmacokinetic studies of different echo-contrast agents in the cerebral circulation of dogs, 1037
Sekhar, L. N., see Dong, M.-L.
Sensier, Y. J. and London, N. J. M.: colour duplex ultrasound assessment of lower limb arterial disease: the effect of adjacent disease, 365 (Letter)

Shadow suppression
spatial compounding in ultrasonic imaging using an articulated scan arm (Hernandez), 229

Shadows
amplitude, isobar and grey-scale imaging of ultrasonic shadows behind rigid, elastic and gaseous spheres (Filipczynski), 261
spatial compounding in ultrasonic imaging using an articulated scan arm (Hernandez), 229

Shankar, P. M., Molthen, R., Narayanan, V. M., Reid, J. M., Genis, V., Forsberg, F., Piccoli, C. W., Lindenmayer, A. E. and Goldberg, B. B.: studies on the use of non-Rayleigh statistics for ultrasonic tissue characterization, 873
Shankar, P. M., see Wu, Y. Q.
Shaw, A., Preston, R. C. and Bacon, D. R.: perfusion corrections for ultrasonic heating in nonperfused media, 203

Shear
imaging of the elastic properties of tissues — a review (Gao), 959

Sheep
downstream determinants of pulsatility of the mean velocity waveform in the umbilical artery as predicted by a computer model (Surat), 707

Sheppard, R. J., see Hughes, S. W.
Shivji, G. S., see Turnbull, D. H.

Shock waves
a new method of quantitative cavitation assessment in the field of a lithotripter (Jöchle), 329
a review of *in vitro* bioeffects of inertial ultrasonic cavitation from a mechanistic perspective (Miller), 1131
a test for cavitation as a mechanism for intestinal hemorrhage in mice exposed to a piezoelectric lithotripter (Dalecki), 493
alteration of cell membrane by stress waves *in vitro* (Lee), 1285
biophysical effects of high-energy pulsed ultrasound on human cells (Feigl), 1267

cell-type-specific response to shock waves of suspended or pelleted cells as analysed by flow cytometry or electrical cell volume determination (Endl), 515
contrast-agent gas bodies enhance hemolysis induced by lithotripter shock waves and high-intensity focused ultrasound in whole blood (Miller), 1089
detection of acoustic emission from cavitation in tissue during clinical extracorporeal lithotripsy (Coleman), 1079
disturbance of cellular calcium homeostasis by *in vitro* application of shock waves (Suhr), 671
physical characteristics and biological effects of laser-induced stress waves (Doukas), 151
the combined effects of high-energy shock waves and ionising radiation on a human bladder cancer cell line (Fickweiler), 1097
the influence of high-energy shock waves on the development of metastases (Oosterhof), 339
the role of cavitation in the induction of cellular DNA damage by ultrasound and lithotripter shock waves *in vitro* (Miller), 681

Shung, K. K., see Chang, P. H.
Shung, K. K., see Wang, S. H.
Shung, K. K., see Wu, S. J.

Simulation
amplitude, isobar and grey-scale imaging of ultrasonic shadows behind rigid, elastic and gaseous spheres (Filipczynski), 261
comparison of Doppler signal analysis techniques for velocity waveform, turbulence and vortex measurement: a simulation study (Wang), 635
computational analysis of the ductus venosus fluid dynamics based on Doppler measurements (Pennati), 1017
downstream determinants of pulsatility of the mean velocity waveform in the umbilical artery as predicted by a computer model (Surat), 707
estimating tissue strain from signal decorrelation using the correlation coefficient (Varghese), 1249
noise reduction in elastograms using temporal stretching with multicompression averaging (Varghese), 1043
particle and voxel approaches for simulating ultrasound backscattering from tissue (Lim), 1237
reduction of stress nonuniformities by apodization of compressor displacement in elastography (Konofagou), 1229
simulation of ultrasonic imaging with linear arrays in causal absorptive media (Berkhoff), 245
the effect of variations in transducer position and sound speed in intravascular ultrasound: a theoretical study (Thompson), 719
two decades of transesophageal phased array probes (Djoa), 1
velocity vector reconstruction for color flow Doppler: experimental evaluation of a new geometrical method (Giarré), 75

Skin
ultrasound backscatter microscope analysis of mouse melanoma progression (Turnbull), 845

Skjoldbye, B., see Holm, H. H.

SMA
changes in superior mesenteric artery Doppler waveform during reduction of cardiac stroke volume and hypotension (Perko), 11
comparison of trans- and intra-abdominal duplex examinations of the splanchnic circulation (Delahunt), 165
pitfalls in the diagnosis of origin stenosis of the coeliac and superior mesenteric arteries with transabdominal colour duplex examination (Geelkerken), 695

Smit, A. J., see Lijmer, J. G.
Smith, J. L., Evans, D. H., Fan, L., Bell, P. R. F. and Naylor, A. R.: differentiation between emboli and artefacts using dual-gated transcranial Doppler ultrasound, 1031
Smith, R. E., see Hussain, S. T.
Smits, G. A. H. J., see Oosterhof, G. O. N.
Sokil-Melgar, J., see Ferrara, K. W.
Sonies, B. C., Wang, C. and Sapper, D. J.: evaluation of normal and abnormal hyoid bone movement during swallowing by use of ultrasound duplex-Doppler imaging, 1169
Sorlie, P., see Li, R.
Spaan, J. A. E., see Bos, L. J.

Species dependence
rabbit and pig lung damage comparison from exposure to continuous wave 30-kHz ultrasound (O'Brien), 345

Speckle reduction
spatial compounding in ultrasonic imaging using an articulated scan arm (Hernandez), 229
the distribution of the local entropy in ultrasound images (Zimmer), 431

Spectral analysis
comparison of Doppler signal analysis techniques for velocity waveform, turbulence and vortex measurement: a simulation study (Wang), 635
differentiation between emboli and artefacts using dual-gated transcranial Doppler ultrasound (Smith), 1031
precision and accuracy of acoustospectrographic parameters (Huisman), 855
quantitative measurements of second harmonic Doppler using ultrasound contrast agents (Chang), 1205
some considerations on the measurements of mean frequency shift and integrated backscatter following administration of Albunex (Wang), 441

Speed of sound
minimal dependence of ultrasonic propagation velocity on frequency (Kohles), 1297 (Letter)
quantitative ultrasonic diagnosis of silicone breast implant rupture: an *in vitro* feasibility study (Forsberg), 53
the effect of variations in transducer position and sound speed in intravascular ultrasound: a theoretical study (Thompson), 719

Spheres
amplitude, isobar and grey-scale imaging of ultrasonic shadows behind rigid, elastic and gaseous spheres (Filipczynski), 261

Spijkerboer, A. M., see Pasterkamp, G.

Splanchnic circulation
comparison of trans- and intra-abdominal duplex examinations of the splanchnic circulation (Delahunt), 165
pitfalls in the diagnosis of origin stenosis of the coeliac and superior mesenteric arteries with transabdominal colour duplex examination (Geelkerken), 695

Spleen
ultrasound-guided spleen biopsy in chimpanzees (pan troglodytes) (Eder), 19

Stadler, R. W., Karl, W. C. and Lees, R. S.: new methods for arterial diameter measurement from B-mode images, 25
Stadler, R. W., Karl, W. C. and Lees, R. S.: the application of echo-tracking methods to endothelium-dependent vasoreactivity and arterial compliance measurements, 35
Stam, C. J., see Keunen, R. W. M.

Standing waves
measurement of antigen concentration by an ultrasound-enhanced latex immunoagglutination assay (Thomas), 1277

van der Steen, A. F. W., see Li, W.
van der Steen, A. F. W., see van Swijndregt, A. D. M.
van der Steen, A. F. W., see Rijsterborgh, H.
Steinbach, P., see Endl, E.
Steinbach, P., see Fickweiler, S.
Stijnen, T., see van der Lugt, A.

Stimulation
application of focused ultrasound for the stimulation of neural structures (Gavrilov), 179

Strain
estimating tissue strain from signal decorrelation using the correlation coefficient (Varghese), 1249
fundamental limitations on the contrast-transfer efficiency in elastography: an analytic study (Kallel), 463
imaging of the elastic properties of tissues — a review (Gao), 959
noise reduction in elastograms using temporal stretching with multicompression averaging (Varghese), 1043
quantitative measurements of second harmonic Doppler using ultrasound contrast agents (Chang), 1205
reduction of stress nonuniformities by apodization of compressor displacement in elastography (Konofagou), 1229

Stress
estimating tissue strain from signal decorrelation using the correlation coefficient (Varghese), 1249
fundamental limitations on the contrast-transfer efficiency in elastography: an analytic study (Kallel), 463
imaging of the elastic properties of tissues — a review (Gao), 959

noise reduction in elastograms using temporal stretching with multicompression averaging (Varghese), 1043
quantitative measurements of second harmonic Doppler using ultrasound contrast agents (Chang), 1205
reduction of stress nonuniformities by apodization of compressor displacement in elastography (Konofagou), 1229

Stress waves
physical characteristics and biological effects of laser-induced stress waves (Doukas), 151

Subarachnoid hemorrhage
an impedance index in normal subjects and in subarachnoid hemorrhage (Giller), 373

Suhr, D., Brümmer, F., Irmer, U. and Hülser, D. F.: disturbance of cellular calcium homeostasis by *in vitro* application of shock waves, 671
Sujana, H., Swamamani, S. and Suresh, S.: application of artificial neural networks for the classification of liver lesions by image texture parameters, 1177
Sung, H.-W., see Cape, E. G.
Surat, D. R. and Adamson, S. L.: downstream determinants of pulsatility of the mean velocity waveform in the umbilical artery as predicted by a computer model, 707
Suresh, S., see Sujana, H.

Surgery
ablation of tissue volumes using high intensity focused ultrasound (Malcolm), 659
interventional ultrasound (Holm), 773
physics of ultrasonic surgery using tissue fragmentation: part I (Cimino), 89
physics of ultrasonic surgery using tissue fragmentation: part II (Bond), 101
potential adverse effects of high-intensity focused ultrasound exposure on blood vessels *in vivo* (Hynynen), 193
the intensity dependence of the site of maximal energy deposition in focused ultrasound surgery (Watkin), 483
ultrasound surgery using multiple sonications — treatment time considerations (Fan), 471

Sutherland, G. R., see Fleming, A. D.

Swallowing
evaluation of normal and abnormal hyoid bone movement during swallowing by use of ultrasound duplex-Doppler imaging (Sonies), 1169

Swarnamani, S., see Sujana, H.
van Swijndregt, A. D. M., The, S. H. K., Gussenhoven, E. J., Lancee, C. T., Rijsterborgh, H., de Groot, E., van der Steen, A. F. W., Bom, N. and Ackerstaff, R. G. A.: an *in vitro* evaluation of the line pattern of the near and far walls of carotid arteries using B-mode ultrasound, 1007

T

Tailor, A., Jurkovic, D., Bourne, T. H., Natucci, M., Collins, W. P. and Campbell, S.: a comparison of intratumoural indices of blood flow velocity and impedance for the diagnosis of ovarian cancer, 837

Tanaka, M., see Sasaki, H.
Tavy, D. L. J., see Keunen, R. W. M.
Taylor, K. J. W., see Holland, C. K.

TCD
an impedance index in normal subjects and in subarachnoid hemorrhage (Giller), 373
diagnosis and follow-up of carotid-cavernous fistulas by carotid duplex sonography and transcranial color Doppler imaging (Chen), 1155
differentiation between emboli and artefacts using dual-gated transcranial Doppler ultrasound (Smith), 1031
nonlinear transcranial Doppler analysis demonstrates age-related changes of cerebral hemodynamics (Keunen), 383
power Doppler: an advance over colour Doppler for transcranial imaging? (Kenton), 313
transcranial Doppler sonography at the early stage of acute central nervous system infections in adults (Müller), 173
transcranial Doppler ultrasonography in neurosurgery: effects of intracranial tumour on right middle cerebral artery flow velocity during induction of anaesthesia (Dong), 1163

TEE
two decades of transesophageal phased array probes (Djoa), 1

Tegeler, C., see Li, R.

Temporal bias
assessment of temporal bias in longitudinal measurements of carotid intimal-medial thickness in the asymptomatic carotid artery progression study (ACAPS) (Riley), 405

Temporal correlation
temporal correlation of blood scattering signals *in vivo* from radiofrequency intravascular ultrasound (Li), 583

Tendon
factors affecting the ultrasonic properties of equine digital flexor tendons (Miles), 907

Tepper, R., see Zimmer, Y.
Terasawa, Y., see Sasaki, H.

Texture analysis
application of artificial neural networks for the classification of liver lesions by image texture parameters (Sujana), 1177

The, S. H. K., see van Swijndregt, A. D. M.

Therapy
ablation of tissue volumes using high intensity focused ultrasound (Malcolm), 659
biophysical effects of high-energy pulsed ultrasound on human cells (Feigl), 1267
potential adverse effects of high-intensity focused ultrasound exposure on blood vessels *in vivo* (Hynynen), 193

the intensity dependence of the site of maximal energy deposition in focused ultrasound surgery (Watkin), 483
ultrasound surgery using multiple sonications — treatment time considerations (Fan), 471

Thermal test objects
perfusion corrections for ultrasonic heating in nonperfused media (Shaw), 203

Thijssen, J. M., see Berkhoff, A. P.
Thijssen, J. M., see Huisman, H. J.
Thomas, N. E. and Coakley, W. T.: measurement of antigen concentration by an ultrasound-enhanced latex immunoagglutination assay, 1277
Thomas, R. M., see Miller, D. L.
Thompson, R. S. and Wilson, L. S.: the effect of variations in transducer position and sound speed in intravascular ultrasound: a theoretical study, 719

Three-dimensional reconstruction
a three-dimensional ultrasound prostrate imaging system (Tong), 735
fetal echocardiography in three and four dimensions (Deng), 979
nearly real-time visualization of arbitrary two-dimensional sections from three-dimensional acquisition (Capineri), 319
observer variability in volumetric blood flow measurements in leg arteries using duplex ultrasound (Hussain), 287
three-dimensional power Doppler imaging: a phantom study to quantify vessel stenosis (Guo), 1059
three-dimensional ultrasonic angiography using power-mode Doppler (Ritchie), 277
ultrasound backscatter microscope analysis of mouse melanoma progression (Turnbull), 845
volume estimation from multiplanar 2D ultrasound images using a remote electromagnetic position and orientation sensor (Hughes), 561

Time-resolved fluorescence imaging
alteration of cell membrane by stress waves *in vitro* (Lee), 1285

Tip vibration
physics of ultrasonic surgery using tissue fragmentation: part II (Bond), 101

Tissue characterisation
an *in vitro* evaluation of the line pattern of the near and far walls of carotid arteries using B-mode ultrasound (van Swijndregt), 1007
analysis of transmural trend of myocardial integrated ultrasonic backscatter in patients with old myocardial infarction (Naito), 807
estimating tissue strain from signal decorrelation using the correlation coefficient (Varghese), 1249
factors affecting the ultrasonic properties of equine digital flexor tendons (Miles), 907
in vitro validation of intravascular ultrasound imaging after balloon angioplasty of coronary artery stenosis (Peters), 999
influence of preload, afterload and contractility on myocardial ultrasonic tissue characterization with integrated backscatter (Naito), 305

influence of tissue preparation on the high-frequency acoustic properties of normal kidney tissue (Sasaki), 1261
particle and voxel approaches for simulating ultrasound backscattering from tissue (Lim), 1237
physics of ultrasonic surgery using tissue fragmentation: part I (Cimino), 89
precision and accuracy of acoustospectrographic parameters (Huisman), 855
real-time assessment of the parameter of nonlinearity in tissue using "nonlinear shadowing" (Fatemi), 1215
studies on the use of non-Rayleigh statistics for ultrasonic tissue characterization (Shankar), 873
ultrasonic measurement of glomerular diameters in normal adult humans (Hall), 987
ultrasonic–pathologic comparison of postangioplasty myointimal hyperplasia and primary atheroma of the superficial femoral artery (Baumgartner), 815

Tissue Doppler imaging
assessment of wall velocity gradient imaging using a test phantom (Nowicki), 1255

Tissue fragmentation
physics of ultrasonic surgery using tissue fragmentation: part I (Cimino), 89
physics of ultrasonic surgery using tissue fragmentation: part II (Bond), 101

Tissue motion
assessment of wall velocity gradient imaging using a test phantom (Nowicki), 1255
imaging of the elastic properties of tissues — a review (Gao), 959

Tissue perfusion
effects of shadowing on the time–intensity curves in contrast echocardiography: a phantom study (Bos), 217
observer variability in volumetric blood flow measurements in leg arteries using duplex ultrasound (Hussain), 287
perfusion corrections for ultrasonic heating in nonperfused media (Shaw), 203
some considerations on the measurements of mean frequency shift and integrated backscatter following administration of Albunex (Wang), 441
subtraction procedure for the registration of tissue perfusion with Doppler ultrasound (Bührer), 651
the relationship between myocardial integrated backscatter, perfusion pressure and wall thickness during isovolumic contraction: an isolated pig heart study (Rijsterborgh), 43
three-dimensional ultrasonic angiography using power-mode Doppler (Ritchie), 277

Tissue preparation
influence of tissue preparation on the high-frequency acoustic properties of normal kidney tissue (Sasaki), 1261

Tissue properties
factors affecting the ultrasonic properties of equine digital flexor tendons (Miles), 907

influence of tissue preparation on the high-frequency acoustic properties of normal kidney tissue (Sasaki), 1261

Tondini, A., see Capineri, L.
Tong, S., Downey, D. B., Cardinal, H. N. and Fenster, A.: a three-dimensional ultrasound prostate imaging system, 735

Transducer
a three-dimensional ultrasound prostate imaging system (Tong), 735
comment on "characterization of ultrasonic transducers using a fiberoptic sensor" (Kwiek), 143 (Letter)
in response to Dr. Kwiek et al. (Wu), 144 (Letter)
physics of ultrasonic surgery using tissue fragmentation: part I (Cimino), 89
physics of ultrasonic surgery using tissue fragmentation: part II (Bond), 101
two decades of transesophageal phased array probes (Djoa), 1
ultrasound surgery using multiple sonications — treatment time considerations (Fan), 471

Transrectal
a three-dimensional ultrasound prostate imaging system (Tong), 735

Tsirulnikov, E. M., see Gavrilov, L. R.
Tu, Y.-K., see Chen, Y.-W.

Tumour detection
application of artificial neural networks for the classification of liver lesions by image texture parameters (Sujana), 1177
imaging of the elastic properties of tissues — a review (Gao), 959
transcranial Doppler ultrasonography in neurosurgery: effects of intracranial tumour on right middle cerebral artery flow velocity during induction of anaesthesia (Dong), 1163

Tumour treatment
the combined effects of high-energy shock waves and ionising radiation on a human bladder cancer cell line (Fickweiler), 1097

Tumour vascularity
a comparison of intratumoural indices of blood flow velocity and impedance for the diagnosis of ovarian cancer (Tailor), 837
correlation of histomorphology of ovarian masses with color Doppler sonography (Fleischer), 555
high resolution 3D color flow mapping: applied to the assessment of breast vasculature (Ferrara), 293
transcranial Doppler ultrasonography in neurosurgery: effects of intracranial tumour on right middle cerebral artery flow velocity during induction of anaesthesia (Dong), 1163

Tunica intima
an *in vitro* evaluation of the line pattern of the near and far walls of carotid arteries using B-mode ultrasound (van Swijndregt), 1007

Tunica media
an *in vitro* evaluation of the line pattern of the near and far walls of carotid arteries using B-mode ultrasound (van Swijndregt), 1007

Turbulence
comparison of Doppler signal analysis techniques for velocity waveform, turbulence and vortex measurement: a simulation study (Wang), 635

Turnbull, D. H., Ramsay, J. A., Shivji, G. S., Bloomfield, T. S., From, L., Sauder, D. N. and Foster, F. S.: ultrasound backscatter microscope analysis of mouse melanoma progression, 845

Two-dimensional reconstruction
nearly real-time visualization of arbitrary two-dimensional sections from three-dimensional acquisition (Capineri), 319

Tymkiewicz, R., see Filipczynski, L.

U

Ultrasonic aspirator
physics of ultrasonic surgery using tissue fragmentation: part I (Cimino), 89
physics of ultrasonic surgery using tissue fragmentation: part II (Bond), 101

Ultrasonic surgery
ablation of tissue volumes using high intensity focused ultrasound (Malcolm), 659
noninvasive arterial occlusion using MRI-guided focused ultrasound (Hynynen), 1071
physics of ultrasonic surgery using tissue fragmentation: Part I (Cimino), 89
physics of ultrasonic surgery using tissue fragmentation: Part II (Bond), 101
potential adverse effects of high-intensity focused ultrasound exposure on blood vessels *in vivo* (Hynynen), 193
the intensity dependence of the site of maximal energy deposition in focused ultrasound surgery (Watkin), 483
ultrasound surgery using multiple sonications — treatment time considerations (Fan), 471

Umbilical artery
development of quantitative Doppler indices for uteroplacental and fetal blood flow during the third trimester (Joern), 823
downstream determinants of pulsatility of the mean velocity waveform in the umbilical artery as predicted by a computer model (Surat), 707

V

Valvular incompetence
accuracy of color Doppler velocity in the flow field proximal to a regurgitant orifice: implications for color Doppler quantitation of valvular incompetence (Perry), 605

Varghese, T. and Ophir, J.: estimating tissue strain from signal decorrelation using the correlation coefficient, 1249
Varghese, T., Ophir, J. and Céspedes, I.: noise reduction in elastograms using temporal stretching with multicompression averaging, 1043

Vascular impedance
a noninvasive method to estimate arterial impedance by means of assessment of local diameter change and the local center-line blood flow velocity using ultrasound (Brands), 895

Vasoreactivity
the application of echo-tracking methods to endothelium-dependent vasoreactivity and arterial compliance measurements (Stadler), 35

Vaughn, A. J., see Delahunt, T. A.

Velocity gradients
assessment of wall velocity gradient imaging using a test phantom (Nowicki), 1255
Verdouw, P. D., see Rijsterborgh, H.

Videodensitometry
effects of shadowing on the time–intensity curves in contrast echocardiography: a phantom study (Bos), 217

Visser, C. A., see Peters, R. J. G.
Vliegen, J. H. R., see Keunen, R. W. M.

Velocity vector
velocity vector reconstruction for color flow Doppler: experimental evaluation of a new geometrical method (Giarré), 75

Völklein, B., see Feigl, T.

Volume measurement
volume estimation from multiplanar 2D ultrasound images using a remote electromagnetic position and orientation sensor (Hughes), 561

Volumetric blood flow
observer variability in volumetric blood flow measurements in leg arteries using duplex ultrasound (Hussain), 287
volumetric flow estimation *in vivo* and *in vitro* using pulsed-Doppler ultrasound (Holland), 591

Vortex
comparison of Doppler signal analysis techniques for velocity waveform, turbulence and vortex measurement: a simulation study (Wang), 635

W

Wall filter
a Doppler ultrasound clutter phantom (Rickey), 747

Wall thickening
the relationship between myocardial integrated backscatter, perfusion pressure and wall thickness during isovolumic contraction: an isolated pig heart study (Rijsterborgh), 43

Wallensteen, M., see Hu, J.
van der Wal, A. C., see Peters, R. J. G.
Wang, A. S., see Dong, M.-L.
Wang, C., see Sonies, B. C.
Wang, S. H., Chang, P. H., Shung, K. K. and Levene, H. B.: some considerations on the measurements of mean frequency shift and integrated backscatter following administration of Albunex, 441

Wang, Y. and Fish, P. J.: comparison of Doppler signal analysis techniques for velocity waveform, turbulence and vortex measurement: a simulation study, 635
Wang, Y. and Fish, P. J.: simulating nonstationary in-phase and quadrature Doppler signals using a time-varying impulse response filter, 529 (Letter)
Watkin, N. A., ter Haar, G. R. and Rivens, I.: the intensity dependence of the site of maximal energy deposition in focused ultrasound surgery, 483

Wavefield extrapolation
amplitude, isobar and grey-scale imaging of ultrasonic shadows behind rigid, elastic and gaseous spheres (Filipczynski), 261
simulation of ultrasonic imaging with linear arrays in causal absorptive media (Berkhoff), 245

Waveform analysis
changes in superior mesenteric artery Doppler waveform during reduction of cardiac stroke volume and hypotension (Perko), 11
development of quantitative Doppler indices for uteroplacental and fetal blood flow during the third trimester (Joern), 823
evaluation of an automated real-time spectral analysis technique (Rickey), 61

Whittle, M.: sonography in obstetrics and gynaecology (5th edition), 949 (Book Review)
Willson, K.: routine checking of ultrasound Doppler devices and routine quality assurance of ultrasound imaging systems, 363 (Book Review)
Wilson, L. S., see Thompson, R. S.
Wójcik, J., see Filipczynski, L.
Wood, R. F. M., see Hussain, S. T.
Wörle, K., see Endl, E.
Wörle, K., see Fickweiler, S.
Wu, S. J. and Shung, K. K.: cyclic variation of Doppler power from whole blood under pulsatile flow, 883
Wu, Y. Q., Shankar, P. M. and Lewin, P. A.: in response to Dr. Kwiek et al., 144 (Letter)

X

Xu, Q., see Deng, C. X.

Y

Yagita, Y., Etani, H., Handa, N., Itoh, T., Imuta, N., Okamoto, M., Matsumoto, M., Kinoshita, N. and Nukada, T.: effect of transcranial Doppler intensity on successful recording in Japanese patients, 701
Yamamoto, K., see Naito, J.
Yambe, T., see Sasaki, H.
Yip, P.-K., see Chen, Y.-W.
Yoganathan, A. P., see Cape, E. G.
Yoganathan, A. P., see Jones, S. A.
Young, R. D., see Miles, C. A.

Z

Zachary, J. F., see O'Brien, W. D., Jr.
Zagar, B., see Ferrara, K. W.

Zhang, H., see Lee, S.
Zhong, M. M., see Chambless, L. E.
Zimmer, Y., Akselrod, S. and Tepper, R.: the distribution of the local entropy in ultrasound images, 431
Zimmer, Y., Tepper, R. and Akselrod, S.: a two-dimensional extension of minimum cross entropy thresholding for the segmentation of ultrasound images, 1183

Send For Your Free Sample Copy Today!

LIFE SCIENCES

Including Pharmacology Letters

Editor-in-Chief
RUBIN BRESSLER, MD
The University of Arizona, Health Sciences Center,
Department of Pharmacology,
1501 North Campbell Avenue, Tucson, AZ 85724, USA

Executive Editor/Europe
SALOMON Z. LANGER, MD
Vice-President, Director of Research,
SYNTHÉLABO Recherche (L.E.R.S.),
92225 Bagneux, France

Co-Editors of **Pharmacology Letters** Section:
ROBERT B. RAFFA, R.W. Johnson, PRI, Spring House, PA, USA
FRANK PORRECA, The University of Arizona Health Sciences Center, Tucson, AZ, USA

LIFE SCIENCES is an international journal publishing full-length reports on research in a range of areas in the life sciences. These areas emphasize the molecular and cellular aspects of: *Cardiovascular & Autonomic Mechanisms; Drug Metabolism; Endocrinology; Growth Factors and Neoplasia; Immunology; Neuroscience; Toxicology*. The Journal publishes original research rapidly – acceptance to publication is just four weeks. In addition to full-length papers, the Journal also features a special section, **Pharmacology Letters**, which includes brief (4 to 6 pages) experimental studies of immediate interest on any aspect of basic pharmacology. **Pharmacology Letters** also offers a rapid publication time of 4 weeks. All papers are rigorously reviewed.

RECENT PAPERS:

T. Ichida, K. Takeda, S. Sasaki, M. Nakagawa, T. Hashimoto, K. Kuriyama, Age-related decrease of γ-aminobutyric acid (GABA) release in brain of spontaneously hypertensive rats.

R. Neubert, N. Hinz, R. Thiel, D. Neubert, Down-regulation of adhesion receptors on cells of primate embryos as a probable mechanism of the teratogenic action of thalidomide.

MINI-REVIEWS:

J.L. Contreras-Vidal, G.E. Stelmach, Effects of Parkinsonism on motor control.

F.J. Dumont, Q. Su, Mechanism of action of the immunosuppressant Rapamycin.

PHARMACOLOGY LETTERS:

D.J. Haleem, A. Yasmeen, M.A. Haleem, A. Zafar, 24h withdrawal following repeated adminstration of caffeine attenuates brain serotonin but not tryptophan in rat brain: Implications for caffeine-induced depression.

G-J. Wang, N.D. Volkow, J.S Fowler, Y-S. Ding, J. Logan, S.J. Gatley, R.R. MacGregor, A.P. Wolfe, Comparison of two PET radiologands for imaging extrastriatal dopamine transporters in human brain.

SUBSCRIPTION INFORMATION:

07538/ISSN: 0024-3205	Volumes 60 & 61, 1997	52 issues per annum
Institutional Rate (1997)		*US$ 3170.00/NLG 5135.00
Personal Rate (1997)		*US$ 344.00/NLG 557.00

(Residents in Colorado and Washington, DC please add appropriate sales tax. Canadian residents please add 7% GST)

NOTE: All subscriptions begin with the first issue of the calendar year and are entered upon receipt of payment. Please allow 4 - 6 weeks for delivery of your first issue. Regular, full price subscription rates are valid until December 31, 1997.

Prices include postage and are subject to change without notice.

*NLG prices apply in Europe, the CIS and Japan. US dollar prices apply to all other customers worldwide.

Life Sciences is indexed/abstracted in:

Current Contents/Life Sciences, Index Medicus, MEDLINE, MEDLARS, CABS, BIOSIS Database, Energy Res Abstr, Energy DataBase, Biological Abstr, Excerpta Medica, Reference Update, Biological and Agricultural Index, Nutrition Abstracts, Ophthal Lit., PASCAL-CNRS Database. PsychINFO, PsychLIT CD-ROM, Psychological Abstracts

In North America: Elsevier Science Inc., Customer Support Dept., PO Box 945, New York, NY 10159-0945
Tel: 212-633-3950 Fax: 212-633-3990 Call toll-free in the USA & Canada: 1-888-437-4636

Outside North America: Elsevier Science, Customer Support Dept., PO Box 211, 1000 AE Amsterdam, The Netherlands
Tel: 31 20 4853 911 Fax: 31 20 4853 598

Nuclear Medicine - and - Biology

- **Radiopharmaceutical Chemistry**
- ***In Vivo* Biochemistry**
- ***In Vivo* Validation Studies**

EDITOR-IN-CHIEF: **WILLIAM C. ECKELMAN,** *Rm 1C-401, Bldg. 10, Clinical Center, NIH, 9000 Rockville Pike, Bethesda, MD, 20892, USA*

AIMS & SCOPE:

Published 8 issues per annum, **Nuclear Medicine and Biology** features original research contributions describing *in vitro* tissue studies and *in vivo* use of radiotracers, radiopharmaceuticals and therapeutic agents. Papers concentrate on the synthesis, testing *in vitro*, and examination of a compound *in vivo*. Extensive studies proving the mechanism of localization *in vivo* whether the radioactive substance is based on receptor-, enzyme-, or tumor antigen-binding or other well defined processes are an integral part of each evaluation. Additionally, studies define a significant compound that is a sensitive probe of a biochemical change *in vivo*.

REVIEW ARTICLES:

K. Nagren, C. Halldin, L. Muller, C-G. Swahn, P. Lehikoinen: Comparison of [11C] methyl triflate and [11C] methyl iodide in the synthesis of PET radioligands such as [11C]B-CIT and [11C]B-CFT.

H.H. Coenen, Dutschka, S.P. Muller, L. Geworski, J. Farahati: N.c.a. radiosynthesis of [123,124I] [Beta]-CIT, plasma analysis and pharmacokinetic studies with SPECT and PET.

O. Ugur, L. Kostakoglu, E.T. Hui, D.R. Fisher, K. Garmestani, O.A. Gansow, N-K.V. Cheung, S.M. Larson: Comparison of the targeting characteristics of various radioimmunoconjugates for radioimmunotherapy of neuroblastoma: Dosimetry calculations incorporating cross organ beta doses.

S.B. Jones, L.J. Tiffany, K. Garmestani, O.A. Gansow, R.W. Kozak: Evaluation of dithiol chelating agents as potential adjuvants for anti-IL-2 receptor lead of bismuth alpha radioimmunotherapy.

D. Gildersleeve, M.E. Van Dort, J.W. Johnson, P.S. Sherman, D.M. Wieland: Synthesis and evaluation of [123I]-iodo-PK11195 for mapping peripheral-type benzodiazepine receptors (omega 3) in heart.

INDEXED/ ABSTRACTED IN:

Current Contents/Life Sciences, Index Medicus, MEDLINE, MEDLARS, Excerpta Medica, CABS, BIOSIS Database, PASCAL/CNRS Database, Applied Health Physics Abstr, Health & Safety Science Abstr, Toxicology Abstracts

SUBSCRIPTION INFORMATION:

07542/ISSN: 0969-8051 Volume 24, 1997 Published 8 issues per year

Personal Rate (1997)	*US$ 199.00/NLG 322.00
Institutional Rate (1997)	*US$ 840.00/NLG 1361.00

(Residents in Colorado and Washington, DC please add appropriate sales tax. Canadian residents please add 7% GST)

NOTE: All subscriptions begin with the first issue of the calendar year and are entered upon receipt of payment. Please allow 4 - 6 weeks for delivery of your first issue. Regular, full price subscription rates are valid until December 31, 1997. Prices include postage and are subject to change without notice.

*NLG prices apply in Europe, the CIS and Japan. US dollar prices apply to all other customers worldwide.

FREE SAMPLE COPY AVAILABLE UPON REQUEST

ELSEVIER SCIENCE

In North America: Elsevier Science Inc., Customer Support Dept., PO Box 945
New York, NY 10159-0945 Tel: 212-633-3950 Fax: 212-633-3990
Call toll-free in the USA & Canada: 1-888-437-4636

Outside North America: Elsevier Science, Customer Support Dept., PO Box 211
1000 AE Amsterdam, The Netherlands
Tel: 31 20 4853 911 Fax: 31 20 4853 598

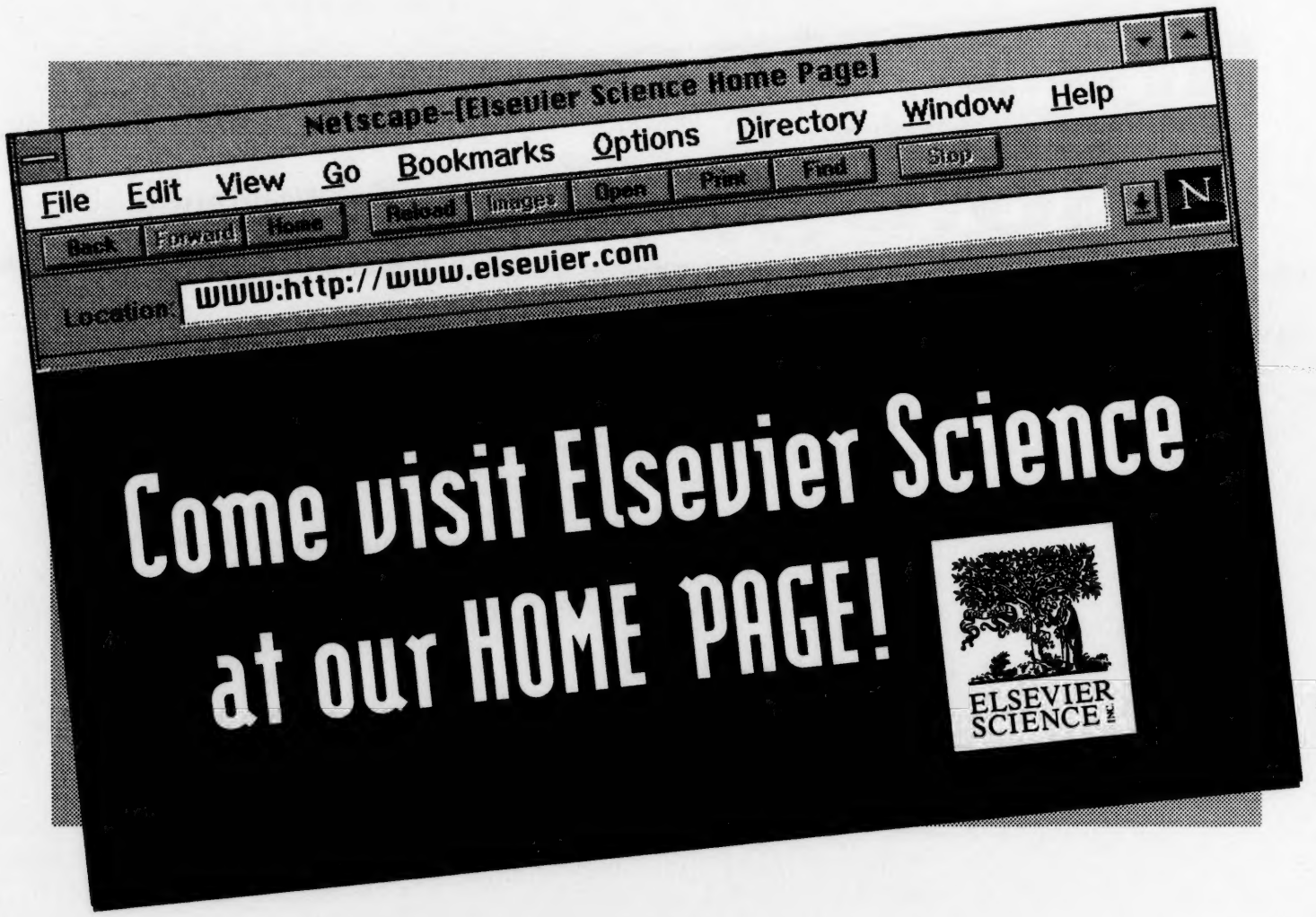
Netscape-[Elsevier Science Home Page]
File Edit View Go Bookmarks Options Directory Window Help
Back Forward Home Reload Images Open Print Find Stop
Location: WWW:http://www.elsevier.com
Come visit Elsevier Science
at our HOME PAGE!
ELSEVIER SCIENCE INC

To find out about the scope of
Elsevier Science publications,
why not access the complete
Catalogue and Publication Home Pages
via the INTERNET:

WWW: http://www.elsevier.com

or

WWW: http://www.elsevier.nl

And check out Elsevier's Database Services and Table of Contents Service.